Human Molecular Genetics, 2015, Vol. 24, No. 5 1441–1456

doi: 10.1093/hmg/ddu561
Advance Access Publication Date: 5 December 2014
Original Article

ORIGINAL ARTICLE

Epigenetic dysregulation of *hairy and enhancer of split 4* (*HES4*) is associated with striatal degeneration in postmortem Huntington brains

Guang Bai[2], Iris Cheung[3], Hennady P. Shulha[4], Joana E. Coelho[1], Ping Li[1], Xianjun Dong[4], Mira Jakovcevski[3], Yumei Wang[1], Anastasia Grigorenko[3], Yan Jiang[6], Andrew Hoss[1], Krupal Patel[2], Ming Zheng[2], Evgeny Rogaev[3], Richard H. Myers[1,5,†], Zhiping Weng[4,†], Schahram Akbarian[3,6,†], and Jiang-Fan Chen[1,*†]

[1]Department of Neurology, Boston University School of Medicine, 715 Albany Street, Boston, MA 02118, USA, [2]Department of Neural and Pain Sciences, University of Maryland Dental School, Baltimore, MD 21201, USA, [3]Brudnick Neuropsychiatric Research Institute, [4]Program in Bioinformatics and Integrative Biology, Department of Biochemistry and Molecular Pharmacology, University of Massachusetts Medical School, Worcester, MA 01604, USA, [5]Genome Science Institute, Boston University School of Medicine, 72 East Concord Street, Boston, MA 02118, USA, and [6]Friedman Brain Institute, Department of Psychiatry, Mount Sinai School of Medicine, New York, NY 10029, USA

*To whom correspondence should be addressed at: Department of Neurology, Boston University, School of Medicine, 715 Albany Street, Boston 02129, MA, USA. Tel: +1 6174141249; Fax: +1 6176385354, Email: chenjf@bu.edu

Abstract

To investigate epigenetic contributions to Huntington's disease (HD) pathogenesis, we carried out genome-wide mapping of the transcriptional mark, trimethyl-histone H3-lysine 4 (H3K4me3) in neuronal nuclei extracted from prefrontal cortex of HD cases and controls using chromatin immunoprecipitation followed by deep-sequencing. Neuron-specific mapping of the genome-wide distribution of H3K4me3 revealed 136 differentially enriched loci associated with genes implicated in neuronal development and neurodegeneration, including *GPR3, TMEM106B, PDIA6* and the Notch signaling genes *hairy and enhancer of split 4* (*HES4*) and *JAGGED2*, supporting the view that the neuronal epigenome is affected in HD. Importantly, loss of H3K4me3 at CpG-rich sequences on the *HES4* promoter was associated with excessive DNA methylation, reduced binding of nuclear proteins to the methylated region and altered expression of *HES4* and *HES4* targeted genes *MASH1* and *P21* involved in striatal development. Moreover, hypermethylation of *HES4* promoter sequences was strikingly correlated with measures of striatal degeneration and age-of-onset in a cohort of 25 HD brains ($r = 0.56$, $P = 0.006$). Lastly, shRNA knockdown of HES4 in human neuroblastoma cells altered MASH1 and P21 mRNA expression and markedly increased mutated HTT-induced aggregates and cell death. These findings, taken together, suggest that epigenetic dysregulation of *HES4* could play a critical role in modifying HD disease pathogenesis and severity.

† These authors jointly directed and contributed equally to this work.

Received: July 1, 2014. **Revised:** October 6, 2014. **Accepted:** November 3, 2014

Introduction

Huntington's disease (HD) is a devastating and progressive neurodegenerative disorder characterized by chorea, dystonia, cognitive impairment and behavioral changes (1,2). The CAG trinucleotide expansion in exon 1 of the huntingtin (*HTT*) gene (3) leads to widespread neuronal loss and gliosis and the appearance of intranuclear inclusions of the mutant huntingtin protein (HTT) in neurons, particularly in the striatum and cerebral cortex. While all HD patients have the same type of mutation (i.e. >35 CAG repeats) which accounts for two-thirds of the variance in age at disease onset, there is significant variation in motor and cognitive symptoms (4,5) and the remaining (one-third) variance of the age-of-onset is likely attributed to other genetic modifier factors (5,6). It is striking that the same genetic (same CAG repeats) architecture is associated with very different age-of-onset, and up to 30-year differences have been reported (5,6). Here, we hypothesize that differences in epigenetic regulation of specific promoter/regulatory sequences influences the degree of striatal degeneration and the disease age-of-onset. Epigenetic mechanisms, including the regulation of DNA methylation and various histone methylation and acetylation markings may contribute to dysregulated transcription, a central feature of HD pathogenesis (7,8). Epigenetic markers in HD may represent novel drug targets for the treatment of HD (9) and other neurodegenerative diseases (10).

Multiple lines of evidence support the possible contribution of epigenetic changes to HD pathogenesis. For example, global levels of histone acetylation are reduced in models of HD (11,12) and in human HD brains (13), and histone hypoacetylation in HD models can be reversed by treatment with histone deacetylase (HDAC) inhibitors which also arrest polyglutamine-dependent neurodegeneration (11) and counteract transcriptional and behavioral changes (14–16). Histone modifications were altered in HTT locus, with increased levels of H3K4 and H3K36 trimethylations and reduced level of H3K9 trimethylation in mouse R6/1 HD model (17). Furthermore, mutant HTT has been shown to interact with proteins for histone methylation, including HYPB, a novel human histone H3 lysine 36-specific methyltransferase associated with active genes (18) and the polycomb repressive complex 2 (*PRC2*), a multi-protein complex with histone methyltransferase activity specific to H3 lysine 27 (H3K27me3) (19). Mutant HTT can induce the repressive histone mark, histone H3 dimethyated at lysine 9 (H3K9me2), by a mechanism involving the transcription of alpha thalassemia/mental retardation X linked (ATRX) (20). In HD striatum, excessive levels of H3K9me2 (21) as well as the reduced level of H3 trimethylated at lysine K4 (H3K4me3) on the promoter for selective sets of the down-regulated genes such as dopamine receptor 2 (*Drd2*) and brain-derived neurotrophic factor (*Bdnf*) (9) have also been reported. However, to the best of our knowledge, no genome-wide study of histone methylation in human HD brains has been undertaken in a cell-type specific manner.

As the first step in probing genome-wide changes of histone methylation markers in HD brains, we mapped the genome-wide distribution of histone H3K4me3 with next generation sequencing technology. The H3K4me3 mark functions as the exclusive docking signal for RNA polymerase II and strongly correlates with activated RNA polymerase II occupancy and transcription rates (22). This epigenetic marker is localized to punctuated sites near the transcription start sites (TSS) of actively transcribed genes (23–26), correlates on a genome-wide scale broadly with gene expression activity, is sharply regulated at TSS and other regulatory sequences associated with the regulation of transcription (27) and may provide novel insights into transcriptional dysregulation in HD. In order to explore the epigenome in the cell type at risk in HD, the cortical and striatal neurons, (28), we employed fluorescent-activated nuclei sorting to isolate neuronal from non-neuronal nuclei residing in the prefrontal cortex (PFC) (29). This enabled a proper comparative analyses of histone marks in neuronal elements, which is an advantage of conventional studies on tissue homogenates because it bypasses the potential confound of degeneration and injury-induced increase in glia-to-neuron ratio (30). Our neuron-specific genome-wide mapping approach identified a large number of epigenetically altered loci in the neuronal *HD* genome, including loss of H3K4me3 and excessive DNA methylation on the *HES4* promoter, as well as altered expression of *HES4* and its target genes Mash1 and p21. We present multiple lines of evidence for a functional role of HES4 in HD pathogenesis, including a significant correlation between *HES4* epigenetic dysregulation and clinical and histopathological parameters as well as mechanistic evidence such as mutant HTT-induced aggregates and cell death after shRNA knockdown of *HES4* in human neuroblastoma cells.

Results

Histone H3K4me3 landscapes in prefrontal neurons of HD and control brains

We mapped the distribution of the H3K4me3 mark, which is sharply enriched around the 5′ end of genes and on a genome-wide scale broadly correlated with gene expression activity, in neuronal chromatin from dorsolateral PFC in six cases and five controls (Table 1). All but one of the HD postmortem brains were collected more than 15 years after onset of HD symptoms (mean = 17.2 years), at which time, striatal neurons would have largely degenerated, resulting in a dramatic decline of neuronal numbers in the caudate nucleus, accompanied by extensive gliosis (30). On the other hand, the PFC of HD brains displays pathological changes similar to the striatum (including mutant HTT aggregation), but with less severe degeneration that defines HD striatum (31,32). Thus, molecular changes detected in HD PFC may be more representative for HD pathology prior to widespread loss of neurons. Consistent with this, the overall FACS sorted $NeuN^+$ cells (per gram tissue) were indistinguishable between HD (4980317 ± 661429) and control brains (5521686 ± 432578) ($P > 0.05$, $n = 12$–15, t-test), indicating that total number of $NeuN^+$ neurons in cerebral cortex was not altered in HD brains.

In our cohort, 85–90% of reads of HD and 82–90% of control cohorts were mapped to one unique location in the genome. Using Poisson statistics (see Materials and Methods) 136 H3K4me3 peaks were identified as differentially distributed between HD and control brain (Supplementary Material, Table S1), with 78 peaks maintaining significance ($P < 0.05$) after correction for False Discovery using the Benjamini and Hochberg method (Table 2). A total of 83 out of 136 peaks were overlapped within 2 kb of a TSS, consistent with previous studies (29,33). For example, there are clear dense H3K4me3 peaks around TSS of the *TTTY15* gene in HD brain (Fig. 1A). Consistent with *TTTY15*'s location on the Y chromosome, there was complete lack of signal in the female sample (HD3584. Fig. 1A). The H3K4me3 distribution was highly consistent among the six HD samples, with >90% overlap with each sample, with few exceptions such as Y-chromosome specific sequences that were limited to male subjects only (Supplementary Material, Table S2).

Among the 136 peaks, 85 peaks were decreased and 51 peaks increased in HD. At least 45 of the 136 peaks as defined by the

Table 1. Demographics of HD and control brains

HD ID	Death	Onset	Duration	CAG repeat size	PMI (h)	Striatal score	Control ID	Death	PMI (h)
(A) Brain samples analyzed for FACS-ChIP-sequencing									
HD-1	55	44	11	45	37	2.66	C-1	55	40
HD-2	56	40	16	45	19	2.66	C-2	56	17
HD-3	71	52	19	43	21	2.43	C-3	71	24
HD-4	69	50	19	42	19	2.48	C-4	69	18
HD-5	43	28	15	49	21	2.70	C-5	43	12
HD-6	68	45	23	42	4	2.67			
(B) Brain samples analyzed for DNA methylation									
HD-2	56	40	16	45	19	2.66	C-7	66	19
HD-3	71	52	19	43	21	2.43	C-8	69	15
HD-4	69	50	19	42	19	2.48	C-9	54	24
HD-5	43	28	15	49	21	2.70	C-10	61	10
HD-6	68	45	23	42	4	2.67	C-12	44	28
HD-7	89	70	19	40	57	3.33	C-13	53	24
HD-8	69	63	6	41	6	2.64	C-14	—	—
HD-9	67	40	27	44	14	3.33	C-15	57	20
HD-10	61	35	26	46	25	3.58	C-16	43	15
HD-11	63	40	23	45	21	2.74	C-17	52	23
HD-12	62	40	22	45	28	3.58	C-18	58	20
HD-13	76	58	18	41	7	—	C-19	70	21
HD-14	48	25	23	48	19	3.82	C-20	46	30
HD-15	40	34	6	51	—	3.52	C-21	66	17
HD-16	55	31	24	47	24	—	C-23	36	21
HD-17	72	55	17	41	8	2.59	C-24	60	24
HD-18	67	48	19	43	22	2.74	C-25	54	24
HD-19	59	35	24	46	6	2.62	C-27	61	17
HD-20	72	55	17	42	12	2.74	C-28	62	18
HD-21	78	62	16	42	18	—	C-29	55	26
HD-22	68	52	16	42	13	2.66	C-30	52	18
HD-23	57	40	17	49	25	2.91	C-31	69	26
HD-24	53	40	13	48	23	3.60	C-32	61	25
HD-25	48	38	10	45	11	3.60	C-33	64	19
HD-26	36	24	12	54	21	2.91	C-34	88	11
							C-35	71	40
							C-36	68	25
(C) Brain samples analyzed for qPCR analysis of mRNA									
HD-2	56	40	16	45	19	2.66	C-10	61	10
HD-3	71	52	19	43	21	2.43	C-11	68	19
HD-4	69	50	19	42	19	2.48	C-12	44	28
HD-5	43	28	15	49	21	2.7	C-13	53	24
HD-6	68	45	23	42	4	2.67	C-15	57	20
HD-8	69	63	6	41	6	2.64	C-18	58	20
HD-16	55	31	24	47	24	—	C-19	70	21
HD-17	72	55	17	41	8	2.59	C-22	73	19
HD-19	59	35	24	46	6	2.62	C-24	60	24
HD-21	78	62	16	42	18	—	C-26	76	26
HD-22	68	52	16	42	13	2.66	C-28	62	18
HD-24	53	40	13	48	23	3.6	C-31	69	26
HD-25	48	38	10	45	11	3.6	C-34	88	11
HD-26	36	24	12	54	21	2.91	C-37	93	13

nearest TSS were associated with neuronal genes important for connectivity and synaptic signaling (e.g. *SHANK3, RIMS2, DLG2/PSD93*) or neuronal transcription (*ARC, RCOR2, MKL1*) (Supplementary Material, Table S1), supporting the view that cortical circuitry is compromised in HD due to widespread alterations in the epigenetic architecture of cortical neurons. Gene ontology (GO) analysis of the 136 peaks, when corrected for multiple comparisons, showed enrichment for eight categories that were overwhelmingly related to neuronal compartments and synaptic signaling (Supplementary Material, Table S3). Notably, six out of eight over-represented GO categories are directly related to synaptic functions, a finding consistent with the fact that we used neuronal nuclei for our ChIP-seq analysis.

Furthermore, 14 of the 78 peaks (after correction of false discovery) altered in HD cortical neurons are ascribed with key roles in neurodegenerative conditions (Supplementary Material, Table S1). These include orphan G protein coupled receptors including *GPR3* modulating gamma-secretase activity and beta-amyloid deposition (34) and *GPR179* which, when mutated, lead to degeneration of bipolar neurons in the retina (35). The list also includes *INF2*, a monogenic cause for Charcot–Marie–Tooth neuropathy (36), *VRK1*, a monogenic cause for progressive

Table 2. H3K4me3 is altered at 78 loci in HD cortical neurons, compared with control neuron

TSS	bp to TSS	Mean CTR	Mean HGT	Log2(CTR/HGT)	P-value (*t*-test)	FDR	Functions
ARC	1715	0.0215	0.0097	2.543	0.0031	0.046	Activity-regulated early response gene with key role in synaptic plasticity
BHLHE40	3320	0.0192	0.0077	1.774	0.0013	0.031	A bHLH transcription factor and key component of the circadian clock
TMEM200B	0	0.0050	0.0124	1.618	0.0011	0.029	
MIR3675	11662	0.0140	0.0041	1.604	0.0035	0.048	
MIR1257	11074	0.0290	0.0140	1.522	0.0004	0.021	
FBXL16	2707	0.0106	0.0042	1.515	0.0001	0.014	
NR4A1	10907	0.0101	0.0045	1.515	0.0000	0.011	Nuclear receptor-related transcription factor implicated in neuroprotection;
SLC22A18	0	0.0105	0.0040	1.508	0.0003	0.018	
DAB2IP	0	0.0111	0.0047	1.448	0.0005	0.023	A GTPase regulator involved in neuronal migration and growth
HBQ1	0	0.0101	0.0035	1.432	0.0001	0.012	
PHLDA2	0	0.0176	0.0080	1.420	0.0010	0.028	
RNF126	3401	0.0126	0.0051	1.376	0.0028	0.043	
BAI1	46840	0.0122	0.0056	1.345	0.0014	0.032	Angiogenesis inhibitor 1, interacts with LRRK2 kinase
CYP2S1	0	0.0184	0.0080	1.333	0.0001	0.014	
LOXL4	0	0.0187	0.0087	1.324	0.0022	0.039	
MIDN	1136	0.0047	0.0126	1.324	0.0007	0.024	Nucleolar protein with ubiquitin-like domain essential for mid-brain development
KIAA1274	0	0.0133	0.0292	1.321	0.0000	0.003	
HES4	0	0.0122	0.0055	1.320	0.0000	0.011	Regulator of neural stem-cell proliferation
FOS	0	0.0325	0.0148	1.320	0.0010	0.029	Early response gene involved in activity-regulated gene expression
RAMP3	0	0.0158	0.0391	1.313	0.0004	0.020	
ETV4	0	0.0243	0.0098	1.307	0.0023	0.040	
INF2	0	0.0235	0.0105	1.306	0.0001	0.013	*Inverted formin*, a monogenic risk gene for Charcot–Marie–Tooth neuropathy
VRK1	235498	0.0108	0.0036	1.305	0.0003	0.018	Monogenic causative gene for postnatal progressive microcephaly syndromes
DSG2	0	0.0159	0.0071	1.296	0.0001	0.011	
BRSK2	19307	0.0190	0.0083	1.293	0.0014	0.033	*BRSK2/SAD defines neuronal polarization and axon growth in cerebral cortex*
NPAS4	0	0.0144	0.0059	1.276	0.0017	0.035	An activity-dependent TF critical for memory and inhibitory synape formation
ADRA1D	0	0.0166	0.0074	1.268	0.0023	0.040	Adrenergic receptor 1D, expressed in forebrain
SLC27A5	1597	0.0123	0.0056	1.265	0.0005	0.023	
PPIC	0	0.0112	0.0048	1.247	0.0001	0.013	
KCNN1	0	0.0188	0.0401	1.237	0.0020	0.037	Calcium-activated potassium channel SK-1, implicated in neuroprotection
GNG13	0	0.0170	0.0391	1.231	0.0017	0.035	
AGRN	12379	0.0118	0.0047	1.224	0.0001	0.014	Synaptogenesis and plasticity in CNS, key neuromuscular junction protein
GOLT1A	62360	0.0174	0.0378	1.216	0.0037	0.049	
SLC26A1	3435	0.0142	0.0305	1.198	0.0010	0.028	
C6orf27	0	0.0145	0.0067	1.196	0.0000	0.011	
JAG2	395	0.0124	0.0056	1.192	0.0001	0.013	Notch receptor ligand Jagged 2, implicated in generation of motor neurons.
HHATL	0	0.0181	0.0066	1.190	0.0014	0.032	
CLEC2L	0	0.0353	0.0165	1.190	0.0000	0.008	
C1orf187	0	0.0139	0.0057	1.179	0.0026	0.042	Neural-specific antagonist to WNT signaling and axon guidance molecule
C19orf26	0	0.0215	0.0075	1.169	0.0010	0.029	
CRHR2	0	0.0252	0.0116	1.167	0.0023	0.039	Corticotropin releasing hormone receptor 2
UNC5A	6354	0.0122	0.0272	1.167	0.0016	0.034	
FLJ37505	424827	0.0214	0.0092	1.166	0.0000	0.001	
AGRN	19672	0.0217	0.0101	1.164	0.0001	0.013	Synaptogenesis and plasticity in CNS, key neuromuscular junction protein
NR4A1	0	0.0110	0.0047	1.163	0.0007	0.026	Nuclear receptor-related transcription factor implicated in neuroprotection
IL2RB	16371	0.0234	0.0094	1.161	0.0034	0.047	

Continued

Table 2. *Continued*

TSS	bp to TSS	Mean CTR	Mean HGT	Log2(CTR/HGT)	P-value (t-test)	FDR	Functions
KIAA0182	146622	0.0219	0.0494	1.155	0.0005	0.022	Interacting with the disrupted in schizophrenia (DISC1) protein
N4BP3	0	0.0173	0.0068	1.145	0.0000	0.009	
TRAF7	2580	0.0126	0.0056	1.144	0.0019	0.037	Encodes TNF receptor-associated protein that regulates apoptosis
MFSD10	0	0.0122	0.0040	1.143	0.0006	0.023	
NCR2	91854	0.0147	0.0064	1.139	0.0008	0.026	
LOC100128338	0	0.0372	0.0149	1.132	0.0000	0.009	
SBK1	30099	0.0111	0.0046	1.132	0.0001	0.014	
PDIA6	23739	0.0192	0.0079	1.129	0.0030	0.045	An isomerase interacting with progranulin, involved in frontotemporal dementia
RCOR2	0	0.0102	0.0041	1.127	0.0001	0.012	Rest Co-repressor 2, chromatin regulator in neuronal progenitor
WTIP	0	0.0100	0.0043	1.119	0.0000	0.009	
LGI2	0	0.0123	0.0053	1.118	0.0001	0.012	
HAGHL	0	0.0119	0.0048	1.115	0.0001	0.012	
LINGO3	0	0.0108	0.0041	1.105	0.0031	0.046	
GPR3	0	0.0148	0.0060	1.103	0.0001	0.012	Orphan GPCR modulating beta-amyloid and neurodegeneration
LOC150381	0	0.0259	0.0115	1.102	0.0000	0.008	
RHBDL1	0	0.0143	0.0064	1.101	0.0010	0.029	
NFIX	0	0.0069	0.0153	1.056	0.0012	0.030	Nuclear protein regulating neural progenitor differentiation in hippocampus
GPM6B	0	0.0121	0.0043	−1.081	0.0009	0.028	
SCN2A	0	0.0121	0.0053	−1.091	0.0009	0.027	Sodium channel and monogenic neurodevelopmental risk gene
CHRNA1	76396	0.0209	0.0096	−1.092	0.0013	0.031	Nicotonic acetylcholine receptor important for axonal development
FLRT3	0	0.0160	0.0056	−1.101	0.0029	0.044	Repulsive axon guidance cue
PDZRN3	62936	0.0074	0.0209	−1.119	0.0003	0.018	
IL1RAPL1	0	0.0163	0.0074	−1.135	0.0009	0.028	IL 1 receptor accessory protein-like 1, a neurodevelopmental risk gene
SPRED2	0	0.0195	0.0033	−1.151	0.0034	0.048	
HMGN4	13970	0.0115	0.0048	−1.156	0.0014	0.032	
MTRF1	0	0.0176	0.0375	−1.171	0.0009	0.028	
COX7B	0	0.0105	0.0039	−1.198	0.0003	0.018	
R3HDM1	54329	0.0118	0.0275	−1.223	0.0020	0.037	
KRT222	0	0.0124	0.0263	−1.305	0.0020	0.038	
SNRPN	382	0.0176	0.0082	−1.322	0.0033	0.047	Small nuclear riboprotein-associated protein N highly expressed in neurons
ANXA1	71133	0.0150	0.0066	−1.431	0.0011	0.030	
ARHGAP21	100221	0.0159	0.0073	−1.500	0.0018	0.036	

postnatal microencephaly syndromes (37) and a transmembraneous protein, *TMEM106B*, implicated in frontotemporal dementia (38,39) and Alzheimer's diseases (40). In addition, multiple H3K4me3 peaks altered in HD neurons are located to the TSSs for genes having a key role in neuronal development and differentiation, such as *TNFRSF18* and *TRAF7*, and for genes encoding two tumor necrosis factor (TNF) receptor-related molecules linked to the neurotrophin BDNF/TRKB signal cascade and developmental regulation of apoptosis (41,42). Notably, *hairy and enhancer of split 4* (*HES4*) and *JAGGED2*, two components of the Notch signaling pathway implicated in the regulation of stem cells and neuronal progenitors (43,44) were identified. For the rest of the study, we focused on the *HES4* epigenetic changes and function in HD for three experimental considerations: (i) our initial screening for 24 genes (randomly selected but with known biological functions related to HD pathogenesis) from 78 genes associated with altered H3K4me3 peaks showed that three genes (including *HES4*) exhibited altered DNA methylation in HD brains; (ii) HES4 mRNA was reduced reportedly by ∼50% in the diseased brains in an earlier transcriptome study on HD brains by Hodges *et al.* (45); and (iii) The *HES* gene family (and more broadly Notch signaling) is recognized for its role in forebrain neuronal development by controlling cell-fate determination in progenitor cells and induction of terminal differentiation (46–48).

HD cortical neurons show selective reduction of *HES4* TSS-associated H3K4me3

Since HTT mutation exists from early development, neurodevelopmental defects have been suggested to contribute to HD pathogenesis (5). Given the recognized role of the HES gene family in development by controlling cell-fate determination in progenitor cells and induction of terminal differentiation (46–48), we performed additional targeted analysis of H3K4me3 signals and

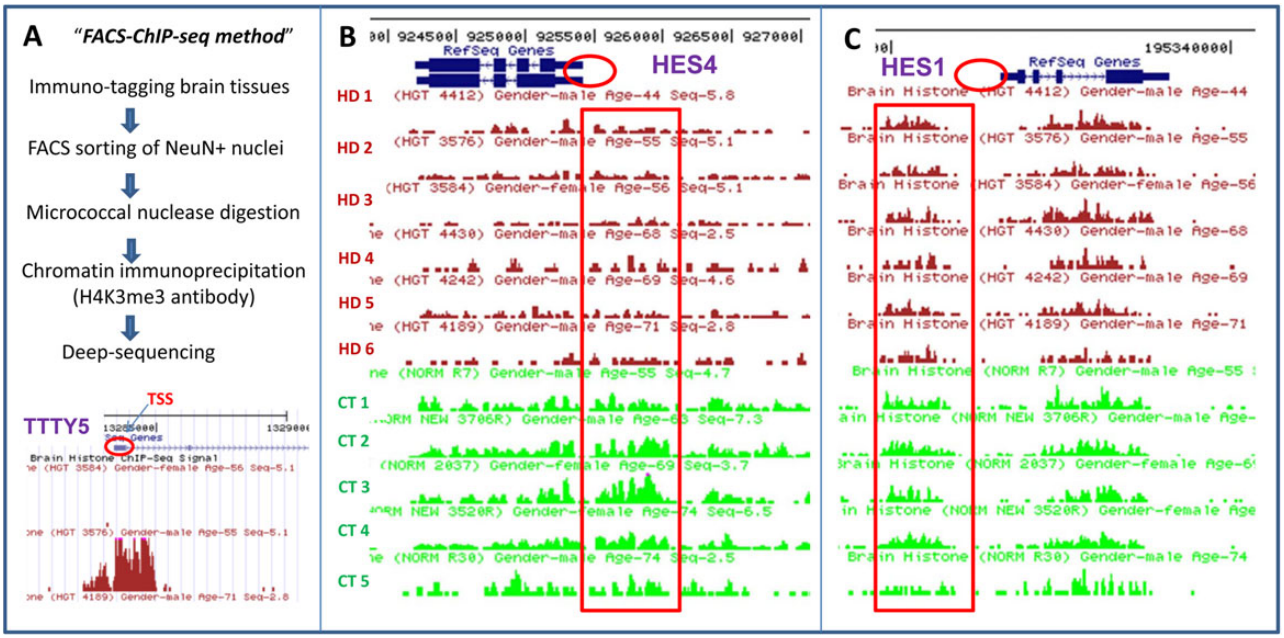

Figure 1. Detection and distribution of H3K4me3 peaks surrounding the *HES4* and *HES1* genes in HD and control subjects. (**A**) Flow chart of the FACS-ChIP-seq procedure as described in the Materials and Methods section for detecting genome-wide distribution of H3K4me3 marks from NeuN$^+$ cortical nuclei of six HD and five control subjects. Low panel: detection of H3K4me3 peak signal for Y chromosome gene *TTTY5* by FACS-ChIP-seq H3K4me3 peaks are distributed in punctuated pattern and highly enriched in TSS of *TTTY5* gene (as indicated by red circle). H3K4me3 peaks surround TTS of *TTTY5* were absent in a female subject (first line) but present in a male sample (second line), confirming specificity of the H3K4me3 peaks detected by FACS-ChIP-seq. (**B**) H3K4me3 peaks were detected by FACS-ChIP-seq in NeuN$^+$ cortical nuclei from six HD and five control subjects as described in the Materials and Methods section. H3K4me3 peaks are clustered around TSS of the *HES4* gene (as indicated red circle). Moreover, the H3K4me3 peak (tag) densities (ad indicated by red long square/box) in HD were lower, compared with controls. (**C**) In contrast, the H3K4me3 peak densities around *HES1* gene were indistinguishable between HD and control subjects.

DNA methylation of the *HES4* gene including its promoter. Figure 1B shows the altered H3K4me3 pattern of *HES4* by FACS-ChIP-seq analysis. The H3K4me3 mark of *HES4* in cortex was increased around the TSS site, while broader regions upstream of the promoter were also involved. As shown in Figure 1, H3K4me3 signals of *HES4* were consistently reduced in all six HD brains compared with all five controls. Total tags of ChIP-seq signal were significantly reduced in HD compared with controls, and statistical analyses of tag densities in HD (0.0077) were statistically different from controls (FDR corrected $P = 0.01$).

Interestingly, the reduced H3K4me3 signal is specific to *HES4* since careful analysis of this histone mark for other genes of the *HES* family (*HES1-HES7*) are not affected, as illustrative by the representative example of *HES1* (Fig. 1C and Supplementary Material, Fig. S1). Recognizing that *HES4* has no direct homologue in the mouse genome, we performed further detailed phylogenetic analysis of *HES4* and *HES* family genes. The *HES4* gene sequences are identified in humans and all analyzed primate species but *HES4* is not specific for primates because close orthologs are found in other mammalian taxons. However, mammalian evolution is associated with occasional and independent losses of *HES4*. For example, rodent *HES4* is lost in the 'mouse-related' clade (*Mus musculus and Rattus norvegicus*), but retained in the 'squirrel-related' clade (*Ictidomys tridecemlineatus*) (see Supplementary Material, Fig. S2A and B).

DNA methylation analysis uncovered an increase in intermediate methylation in the HES4 gene in HD brains

In consideration of the relationship between H3K4me3 and DNA methylation (49), we examined *HES4* DNA methylation using the SABiosciences/Qiagen Methyl-Profiler method which assessed unmethylated (UM), fully methylated (FM) DNA and intermediately methylated (IM) DNA representing monoallelic DNA methylation as well as partial DNA methylation on one or both strands. We assessed DNA methylation states of selected CpG islands (CGIs) in the PFC of 27 control and 25 HD brains (Table 1B). Figure 2A shows examples of qPCR curves of all four reactions in one control (left) and in one HD (right) sample for *HES4*. The analysis showed that in the control brain, the *HES4* promoter was largely unmethylated (~95%, Fig. 2B, left panel), but in HD brain, the UM fraction in *HES4* was significantly reduced (Fig. 2B, $P < 0.01$) and mostly converted to IM making the IM fraction significantly higher ($P < 0.001$) in HD. Specifically, IM is robustly increased from 5% of total input DNA in control to 49% in HD (Fig. 2B, right panel), indicating that most DNA methylation occurs heterogeneously on individual molecules. In contrast, FM of *HES4* was not altered. After cloning the qPCR product from the DNA methylation assay, we obtained the sequence of this 269-bp fragment in the *HES4* promoter, in which 33 CpG dinucleotides were identified on each strand proximate to the TSS (Fig. 2, upper, right panel).

Nuclear proteins binding to the *HES4* promoter are reduced after DNA hypermethylation in *vitro*

Dysfunctional transcription in HD may be associated either with altered DNA methylation in HTT-targeted gene promoters, or altered nuclear proteins that bind to these HTT-targeted gene promoters, or both. While Figure 2 indicates altered DNA methylation in the *HES4* promoter, the abnormality of nuclear proteins in HD may play a role in altered transcription. To address this issue, we performed an electrophoretic mobility shift assay (EMSA) to analyze the interaction of nuclear proteins with this

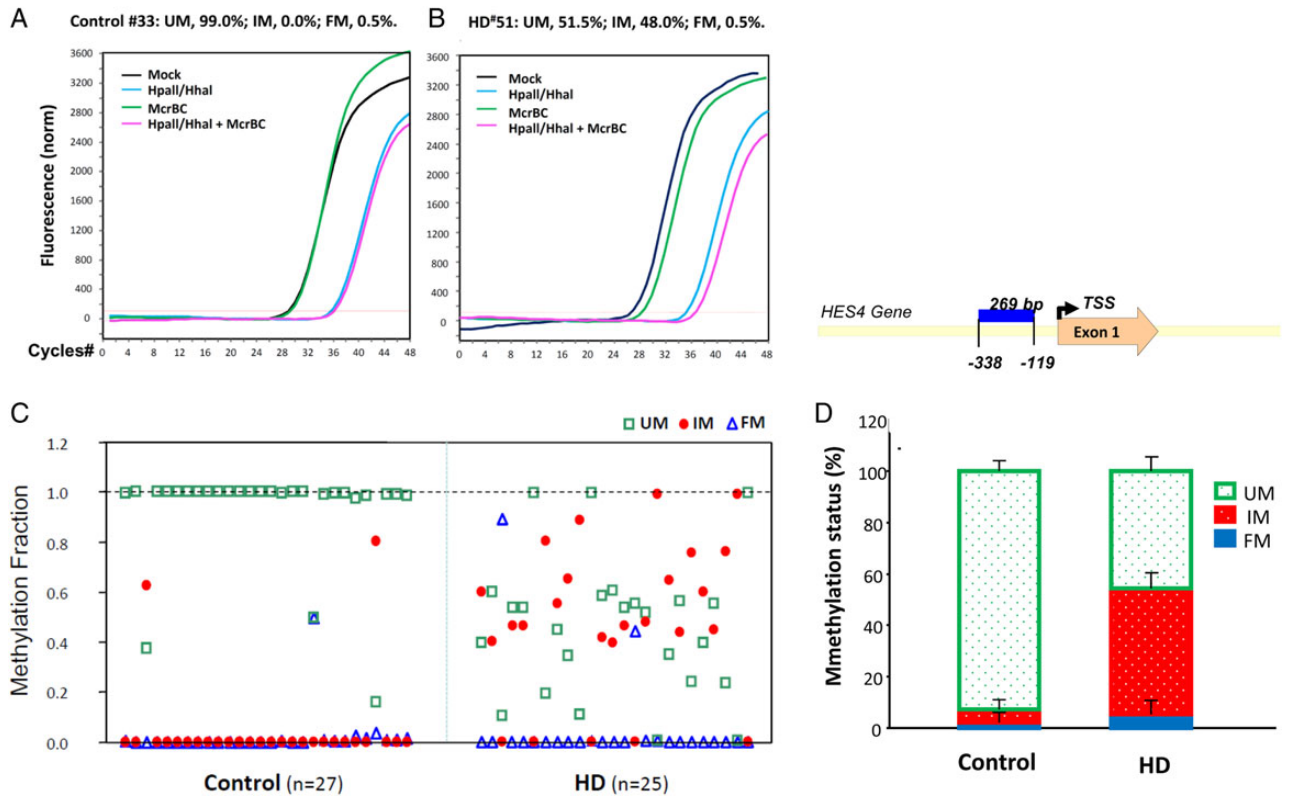

Figure 2. DNA methylation of the *HES4* promoter of HD and control cortex. DNA methylation states of a 269-bp fragment of the *HES4* promoter in the PFC of 27 controls and 25 HD were measured by Methyl-Profiler as described in the Materials and Methods section. (Left) Examples of qPCR curves of all four reactions in one control and in one HD for the *HES4* gene. DNA methylation states for the *HES4* promoter are expressed as fractions of unmethylated (UM), intermediate-methylated (IM) or fully methylated (FM) DNA. (Right) IM was robustly increased from 5% of total input DNA in control to 49% in HD while UM fraction in the *HES4* promoter was reduced in HD. In contrast, FM of the *HES4* gene did not exhibit significant change.

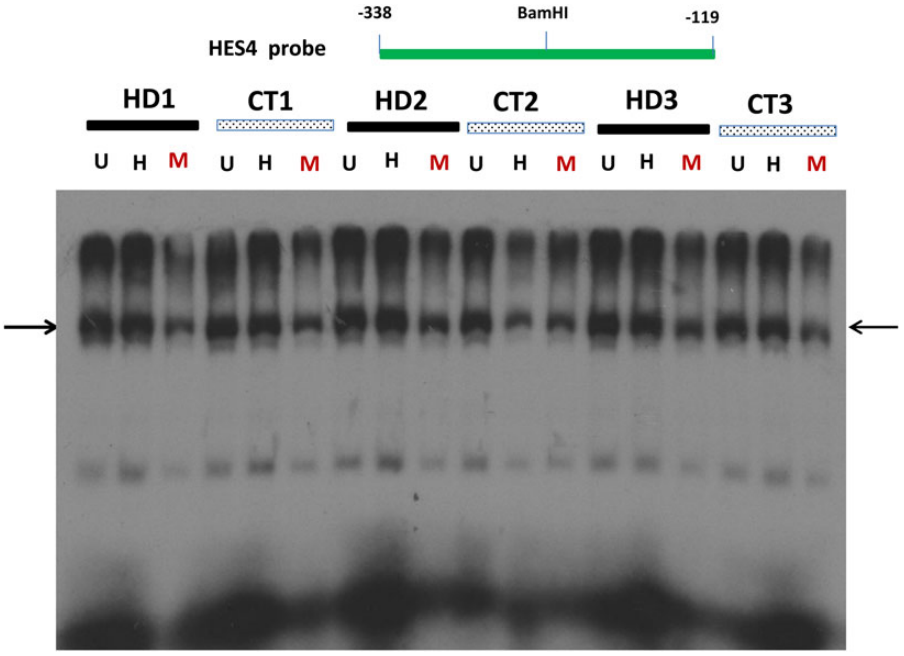

Figure 3. The binding of nuclear proteins to the *HES4* promoter is reduced after DNA hypermethylation *in vitro*. Binding of nuclear proteins from HD and control cortex to the 269-bp fragment of the *HES4* promoter with *in vitro* DNA methylation by EMSA as described in the Materials and Methods section. This 269-bp fragment of the *HES4* promoter was first digested *Bam*HI into two identical DNA fragments and *in vitro* methylated and then re-annealed unmethylated (U), fully methylated (M) and hemi-methylated (H) double strand DNA probes for EMSA. Note that nuclear protein binding (indicated by arrows) was reduced and shifted to high molecular weight band at the fully methylated *HES4* promoter compared with the un-methylated or hemi-methylated *HES4* promoter.

269-bp fragment of the *HES4* promoter (−338 to −119 bp upstream of TSS) after *in vitro* methylation. Since we cannot completely reproduce the DNA methylation status observed in human post-mortem brains, we used double-stranded DNA fragment of the *HES4* promoter as probes under conditions of non-methylation, hemi-methylation and full methylation to partially capture DNA methylation status. We tested unmethylated (U, both strands unmethylated), hemi-methylated (H, one strand methylated and other unmethylated) and fully methylated (M, both strands methylated) DNA in EMSA. Multiple bands were formed between nuclear proteins and the *HES4* promoter fragment (Fig. 3). Interestingly, nuclear protein binding was significantly lower in all bands formed with the fully methylated *HES4* promoter, compared with the unmethylated or hemi-methylated *HES4* promoter, consistent with the notion that altered DNA methylation can affect nuclear proteins binding to the *HES4* promoter. However, the binding to individual probes was indistinguishable between HD and control brains, indicating that there was no abnormality of nuclear proteins that bind to the *HES4* promoter. Taken together with Figure 2 (increased DNA methylation) and 3 (reduced nuclear protein binding to fully methylated probe), it is likely that the DNA methylation status, but not the quality or quantity of nuclear proteins, may contribute to dysfunctional transcription in HD brains.

The mRNA levels for *HES4* and two down-stream target genes, *Mash1* and *p21*, are reduced in HD versus control PFC

To examine the functional impact of the *HES4* promoter IM increase, we determined the mRNA levels for *HES4* in cortex by qPCR analysis in 14 HD and 14 control PFC samples (Table 1C) and found that HES4 mRNA is reduced ∼40% in HD cortex compared with control (Fig. 4A) (*t*-test, $P < 0.05$). This finding is consistent with an earlier transcriptome study in HD, with ∼50% reduction of HES4 mRNA in the diseased brains (45). Consistent with the strong H3K4me3 peaks associated with *HES4* in NeuN$^+$ nuclei, qPCR analysis of FACS sorted cells showed that HES4 mRNA was significantly enriched in neuronal (NeuN$^+$) nuclei compared with non-neuronal (NeuN$^-$) nuclei in human cortex, (Fig. 4B). Moreover, this decrease in HES4 mRNA is also consistent with the reduction in nuclear protein binding to fully methylated DNA, probably due to increased IM of symmetric and incomplete methylation of the *HES4* promoter in HD brain. Considering that HES1 positively regulates expression of *MASH1* (a proneuronal, forebrain-specific transcription factor) (50) and negatively regulates *P21* (a cell cycle suppressor) (51–53), and that HES proteins share certain structural motifs (54), we hypothesized that HES4 modulates these HES targeted gene expression as *MASH1* and P21. Indeed, our qRT–PCR results showed that the reduced HES4 mRNA was associated with down-regulation of MASH1 mRNA in HD cortex compared with the control. In contrast, P21 mRNA was increased in the cortex of HD compared with the control. Therefore, HES4 and its targeted genes *MASH1* and *P21* may play a role in the neurodegeneration of HD.

The extent of intermediate DNA methylation of the *HES4* promoter is correlated with striatal degeneration and with age-of-onset in HD

The correlation of levels of un-methylated, intermediate methylation and hyper-methylation to the characteristics of the HD samples is presented in Table 3. The levels of FM and UM sites were not significantly correlated with any of the HD sample characteristics. The level of intermediate methylation was correlated with the level of striatal involvement ($r = 0.56$, $P = 0.006$) and was also correlated with the age at death ($r = -0.47$, $P = 0.02$), age at onset ($r = -0.48$, $P = 0.02$) and the size of the HD CAG repeat ($r = 0.50$, $P = 0.01$). The correlation between intermediate methylation and striatal involvement remained after removing the four samples with no intermediate methylation ($r = 0.50$, $P = 0.02$). No differences were seen between the HD cases and controls for age at death ($t = -0.81$, $P = 0.42$) or PMI ($t = 1.21$, $P = 0.23$).

Because the intermediate methylation level was correlated with several different features of the HD samples, we sought to assess the main effect of the level of striatal involvement by multivariate analysis of the relationship of the level of intermediate methylation, controlling for the age-at-onset, the size of the HD repeat and the level of cortical involvement. The relationship of intermediate methylation to striatal involvement remained after adjustment for these other factors. Similar results were found consistently with other models including the level of cortical involvement or when removing onset age to avoid over parameterization.

shRNA knockdown of *HES4* in human neuroblastoma cells alters MASH1 and P21 mRNA, and markedly increases mutant HTT-mediated aggregates and cell death

To probe a functional role of HES4 in development of mutant HTT-induced pathology, we further investigated the effect of shRNA-mediated knockdown of HES4 on mutant HTT-induced aggregates and cell deaths in human neuroblastoma HTB-11 cells. The effectiveness of shRNA-HES4 was confirmed by reduction of HES4 mRNA by ∼70% in cells transfected with shRNA-HES4-1 (selected from four distinct shRNAs against HES4) compared with cells transfected with shRNA-control (Fig. 5B). Furthermore, MASH1 mRNA was down-regulated and P21 mRNA was upregulated by *HES4* knockdown with cognate shRNA while scramble (sc) shRNA did not alter these mRNAs (Fig. 5B). Thus, *HES4* exerted similar control of the down-stream targeted gene, *MASH1* and *P21* in both mature neuron in the HD brain (Fig. 4) and cultured HTB-11 neuroblastoma cells.

Next, we evaluated the effect of shRNA-HES4-1 on mutant *HTT*-induced aggregates by immunohistochemistry. After co-transfection of shRNA-HES4-1 or control vector across three concentrations of *HTT* (0.5, 1.0 and 2.0 μg) with three different CAG repeats (23, 73 and 145 CAG repeats, Q23, Q73 and Q145, respectively), we found that co-transfection of shRNA-HES4-1 and *HTT*-Q145 (2.0 μg) produced highly dense nuclear aggregates with little effect of shRNA1-HES4-1 or *HTT*-Q145 alone compared with the cells transfected with sc shRNA /pcDNA3 (Fig. 5A). Quantitative evaluations of the relative size of cellular aggregates and the density of aggregation using an automated image analysis revealed that cells co-transfected with *HTT*-Q145 plus HES4 shRNA had significantly higher percent aggregation area than cell co-transfected with the *HTT*-Q145 plus sc shRNA (5.26% versus 0.75%; $P = 0.002$) while the density of aggregates were unaffected ($P = 0.09$) (Fig. 5C). The similar exacerbated effect was observed in *HTT-Q73* transfected cells, which exhibited a significant increase in aggregation in cells co-transfected with HES4 shRNA compared with that co-transfected with sc shRNA (2.44% versus 0.82%, $P = 0.02$) but there was no significant change in aggregate density between the cells co-transfected with HES4 shRNA or sc shRNA ($P = 0.99$) (Fig. 5C). There was no significant

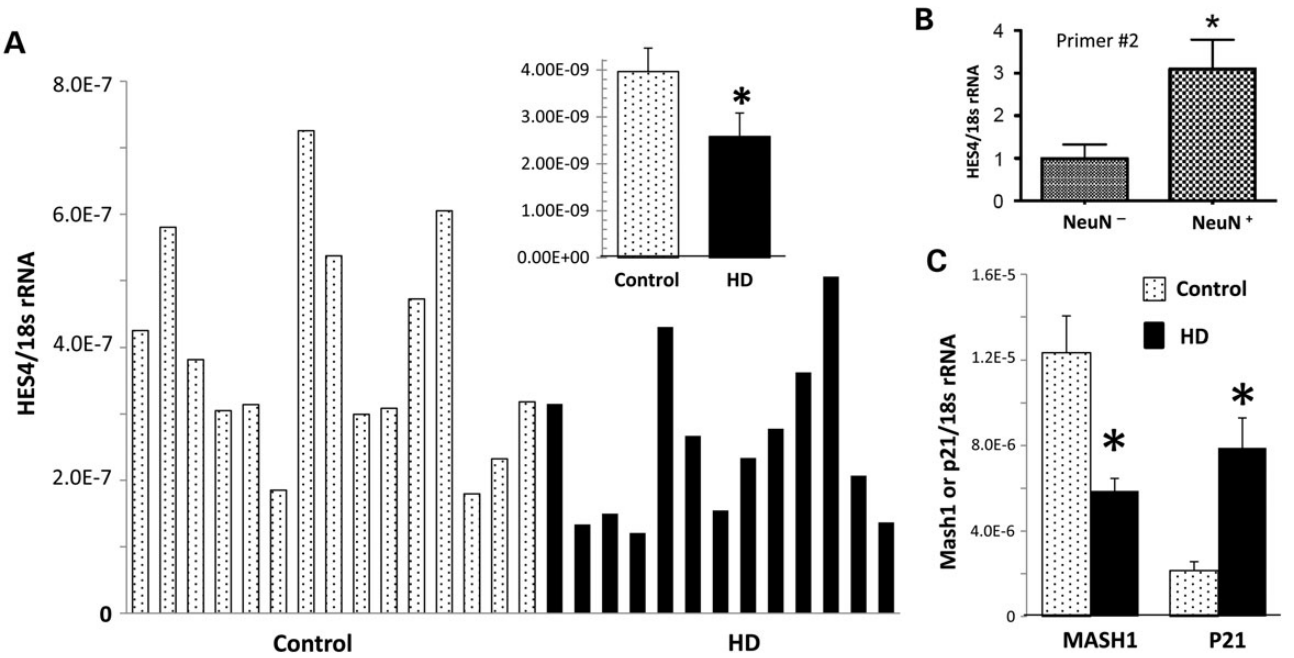

Figure 4. The mRNA levels for HES4 as well as two down-stream target genes, MASH1 and P21, are reduced in the cortex of HD compared with controls. mRNA levels for HES4 (**A**) and its down-stream target MASH1 and P21 (**C**) in total cortex tissues were detected by qPCR analysis as described in the Materials and Methods section. We also measured relative heterogenous nuclear HES4 mRNA levels in NeuN$^-$ and NeuN$^+$ nuclei FACS sorted from human brains using two different primer sets [primer #2, (**B**) and primer #3 (data not shown]. (A) HES4 mRNA is reduced ∼40% in HD cortex compared with control. (B) HES4 mRNA is enriched in human neuronal nuclei ($N = 3$, $P = 0.05$, Mann–Whitney, one-tailed). (**C**) MASH1 mRNA in HD cortex compared with the control while P21 mRNA was increased in the cortex of HD compared with control. *$P < 0.05$ ($n = 14$, t-test). All data are presented as relative ratio of targeted mRNA over 18s rRNA, and presented as mean ± SEM.

Table 3. Spearman correlation of methylation levels of the HES4 promoter with HD sample characteristics

	Hyper-methylation	Intermediate methylation	Un-methylated
Striatal involvement	−0.22	0.56	−0.36
P-value	0.32	0.006	0.10
n	22	22	22
Cortical involvement	−0.33	0.09	0.06
P-value	0.13	0.69	0.79
n	22	22	22
Onset age	−0.037	−0.48	0.39
P-value	0.87	0.02	0.0661
n	23	23	23
HD CAG repeat	−0.15	0.50	−0.35
P-value	0.47	0.01	0.08
n	25	25	25

effect of HES4 shRNA on HTT aggregates in cells transfected with *HTT*-Q23 or cells transfected with pcDNA3 vector.

Lastly, we evaluated the effect of shRNA-HES4-1 on *HTT*-induced cell death by trypan blue exclusion assay. Transfection of shRNA-HES4-1 or *HTT*-Q145 individually did not significantly affect cell death rate, but co-transfection of shRNA-HES4-1 and *HTT*-Q145 increased cell death rates by ∼3-folds compared with the pcDNA3-sc shRNA (Fig. 5D). This effect was selective for *HTT*-Q145 since co-transfection of shRNA-HES4-1 and *HTT*-Q23 did not affect the cell-death rate. Thus, down-regulation of HES4 by shRNA selectively increased *HTT*-Q145-induced ubiquitin-positive aggregates and cell death in HTB-11 cells. These findings support a pathological potential for HES4 in control of mutant *HTT*-induced HD pathogenesis.

Discussion

Transcriptional dysregulation is a central and early feature of HD pathogenesis, and includes a number of post-translational histone modifications (10,55,56). While histone acetylation is generally associated with open chromatin and active transcription, histone methylation is dependent on histone residue, degree of methylation (mono-, di- and tri-) and also specific gene locus and local chromatin environment, associated with repressive or facilitative effector proteins for the process of gene expression. For example, overall levels of a repressive mark, histone H3 trimethylated at lysine 9 (H3K9me3) and expression of H3K9 methyltransferase gene, *ESET/SETDB1*, are reportedly increased in HD patients and in transgenic R6/2 HD mice (21). Down-regulation of *ESET* expression and H3K9me3 by treatment with mithramycin and cystamine significantly ameliorated the behavioral and neuropathological phenotypes of R6/2 mice and extended survival by over 40% (57). A recent study in HD frontal cortex and striatal tissue extracts showed that H3K4me3 alterations at candidate gene promoters with down-regulated expression, including dopamine receptor 2 (*DRD2*), preproenkephalin (*Penk1*), brain-derived neurotrophic factor (*BDNF*) and synaptophysin (*Syp*) (9). To the best of our knowledge, our study is the first to embark on genome-scale unbiased mapping of H3K4me3 in a cell-type specific manner (FACS-sorted cortical neuronal nuclei) from postmortem HD and control brain. Consistent with H3K4me3 as a fingerprint for actively transcribed genes and a marker for transcription initiation sites (23–26), majority (83 out of 136) H3K4me3 peaks were mapped to genome

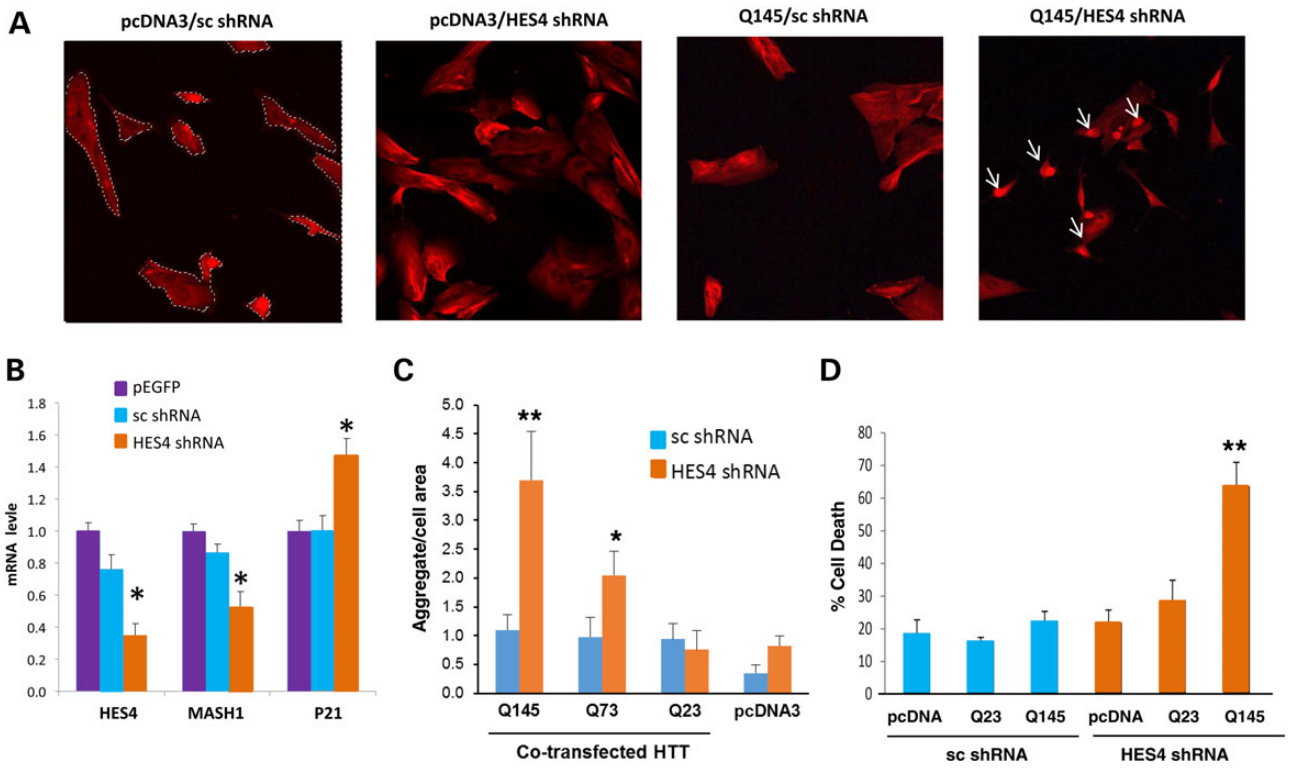

Figure 5. shRNA knockdown of HES4 in human neuroblastoma cells alters mRNA levels of HES4, MASH1 and P21, and markedly increases mutant HTT-induced aggregates and cell death. HTB-11 cells were transfected with shRNA-HES4-1 or sc shRNA with or without different (23, 73 and 145) CAG repeats (*HTT*-Q23, *HTT*-Q73 and *HTT*-Q145), and qRT–PCR analysis, immunohistochemistry and cell death assays were performed as described in the Materials and Methods. (**A**) Ubiquitin immunohistochemistry showed that co-transfection of shRNA-HES4-1 and mutant *HTT*-Q145 for 24 h produced highly dense protein aggregates (aggregates = white arrow, cellular area = dash line) with no effect of shRNA-HES4-1 or *HTT*-Q145 alone compared with the cells transfected with shNRA-control/pcDNA3. (**B**) Quantitative analyses of HES4, MASH1 and P21 mRNAs in HBT-11 cells transfected with EGFP, sc shRNA or HES4-1 shRNA. Data are presented as mean values (plus s.e. from six transfection) of fold change relative to cells receiving EGFP after normalized to 18 s rRNA. HES4 shRNA decreased HES4 mRNA by ~70%, MASH1 mRNA by ~50% and increased P21 mRNA by ~40%, compared with the sc shRNA. (**C**) Exacerbated HTT aggregates by shRNA knockdown of HES4 mRNA in HTB-11 cells. Cells were ubiquitin stained to detect the protein aggregation which was measured using automated image analysis as described in the Materials and Methods. Co-transfection of HES4 shRNA exacerbated *HTT* Q145-, *Q73*- (but not *Q23*-) induced cellular aggregates, as evident by increased relative size of cellular aggregates, in HTB-11 cells. (**D**) Trypan blue exclusion assay showed that shRNA-HES4-1 or *HTT*-Q145 alone did not have significant effect on cell death, but co-transfection of shRNA-HES4-1 and Q145 increased cell death rates compared with shRNA-control. $^{**}P < 0.01$, Student's *t*-test or One-way ANOVA, *post-hoc* Dunn's test (B–D).

positions within 2 kb of a TSS, with the highest peaks around 100 bp downstream of the TSS in both HD or control brains. Thus, mutant HTT protein is unlikely to be associated with a generalized distortion of histone methylation landscapes in diseased neurons. Instead, HD appears to be associated with highly specific defects at (according to our estimates) 78 loci (after correction for false discovery) in various portions of the genome. There was a striking enrichment for genes defining neuronal function and synaptic signaling (Table 2), confirming that the molecular pathology of HD is associated with severe defects in cortical neurons (58). At some of these loci, including the *HES4* promoter, multiple types of epigenetic markings showed disease-associated changes, including DNA cytosine methylation which generally shows an opposing and largely non-overlapping distribution with H3K4me3. Importantly, altered H3K4me3 signaling in HD may relate to a strong inverse correlation between DNA methylation and the presence of H3K4me3 (49). Unmethylated CGIs have been shown to recruit the CxxC finger protein 1 (Cfp1) that associate with the H3K4 methyltransferase Setd1 (Set1/COMPASS or Set1B) (59,60) to create chromatin domains rich in H3K4me3 for enhanced gene expression (61). This is consistent with our finding that the reduced H3K4me3 signal for *HES4* is associated with increased DNA methylation in the *HES4* promoter. Furthermore, recent studies have demonstrated that normal *HTT* function facilitates epigenetic silencer polycomb repressive complex 2 (PRC2) which regulates methylation at histone H3-lysine 27 (19). Since H3K4me3 demethylase, namely Rbp2 (KDM5A or *JARID1A*), is recruited by PRC2 (62), mutant HTT may reduce H3K4me3 signaling by facilitating PCR2 function. In particular, a recent study by Vashishtha *et al.* (9) showed that knockdown of H3K4 demethylase SMCX/Jarid1c by shRNA in primary neurons reverses some of the down-regulation of key neuronal genes by HTT, such as *BDNF*. Furthermore, there is evidence for physical interactions, and functional crosstalk, between histone deacetylases and histone demethylases in intact cells (63,64). The Class I-specific HDAC inhibitors increase in histone acetylation as well as H3K4me2/H3K4me3 levels in cortical neurons and astrocytes (65). Since global levels of histone acetylation are reduced in models of HD (11,12) and HD brains (13), reduced histone acetylation by mutant HTT may also reduce H3K4me3. Thus, mutant HTT may specifically interact with molecules that regulate DNA methylation (CFP1) or histone methyltransferases associated with trithorax (TRXG) or polycomb 2 (PRC2) chromatin remodeling complexes, or HDAC to increase DNA methylation and reduce H3K4me2/3 in the *HES4* promoter and a select subset of additional promoters and regulatory DNA sequences in HD cortical neurons. The alteration of H3K4me3 may directly (by interacting with histone modification enzymes such as PRC2 or Jarid1c, or

indirectly by affecting chromatin structures and chromatin remodeling in general) produce HTT-induced transcriptional changes.

The involvements of the HES family in HD pathogenesis are largely unknown. Our finding of reduced H3K4me3 level, increased DNA methylation of the *HES4* promoter and reduced HES4 mRNA levels in HD cortical neurons and increased mutant HTT-induced aggregates and cell death following shRNA knockdown of HES4 in human neuroblastoma cells provide evidence potentially linking the HES transcription factor family to HD pathogenesis. Interestingly, reduced H3K4me3 is specific for *HES4* since analysis of this histone mark for other HES family members shows no significant changes. The *HES4* gene, while present in many vertebrate genomes, is not found in *Muridae* (including mouse and rat) genomes. However, extensive cortical dysfunction in HD mouse models was noted, other notch signaling pathway (e.g. mouse *Hes1*, most closely related mouse homology to *HES4* in human) may compensate for the dysfunction of *HES4*. HES4 mRNA is also significantly enriched in human neuronal nuclei as one of heterogeneous nuclear RNAs (Fig. 4B), raising a possibility of the involvement of hnHES4 RNA in transcriptional regulation and RNA processing. Importantly, we observed that a significant increase in intermediate methylated DNA of the *HES4* promoter occurred in HD brain and this increase is associated with the reduced nuclear protein binding to the fully methylated *HES4* promoter compared with the un-methylated or hemi-methylated *HES4* promoter. It is likely that the increased intermediately methylated DNA (but not hemi-methylated DNA with only one strand methylated (66) can be attributed to increased asymmetric semi-methylation in HD in view of the similarity of its protein binding pattern to un-methylated and hemi-methylated DNA (Fig. 3). This type of asymmetric semi-DNA methylation is a mechanism that may be particular relevant in differentiated tissues in the context of disease (67,68), in contrast to hemimethylation which commonly is linked to the process of DNA replication. In HD brain, DNA methylation in the *HES4* promoter, instead of alterations in nuclear protein function, is a key player in downregulating HES4 mRNA.

In addition to the altered epigenetic modifications of *HES4* and reduced *HES4* mRNA, our analysis uncovered that two HES4 targeted genes, MASH1 and P21, were dysregulated in HD cortex in opposite directions, down-regulation of MASH1 and up-regulation of P21. The opposite regulations of HES4 target genes were further confirmed by shRNA knockdown of HES4 in cultured neuroblastoma (Fig. 5A). Mash1 is a forebrain neuronal transcription factor and is critically involved in striatal development (46,50). HES4 can suppress MASH1 expression by disrupting the formation of E47 with the striatum-specific bHLH factor Mash1; *HES4* can also interact with the Orange domain to remove the repression of transcription of *P21*. Blocking *Hes1* (the closest rodent HES family to human *HES4*) expression stimulates the expression of cyclin-dependent kinase inhibitor P21 and modulates differentiation of GABAergic (striatal) neurons (51). Thus, the coordinate interplay of HES family proteins and its down-stream targets *MASH1* and *P21* play a critical role in guiding the phenotypic development of striatal GABAergic neurons. Thus, epigenetic changes of *HES4* (i.e. reduced H3K4me3 signal and increased DNA methylation on the *HES4* promoter) led to lower *HES4* expression and dysregulation of putative *HES4* target genes, including *MASH1* and *P21*, to affect forebrain neuronal development and contribute to HD pathogenesis (69). Given the critical role of Notch signaling in forebrain neuronal development, the finding of dysregulated epigenetic modifications of *HES4* and altered expression of Notch signaling molecules (MASH1 and P21) is consistent with the notion that HD may be a lifelong disease process (69) and suggests that abnormal neurodevelopment involving Notch signaling may contribute to HD pathogenesis.

The significance of epigenetic modifications of the *HES4* function is substantiated by the finding that the degree of DNA methylation of the *HES4* promoter is associated with striatal degeneration and age of onset of HD patients. Recently, we uncovered, among 523 HD patients, two classes of HD pathology with mainly striatal degeneration (class I) or cortical degeneration (class II) (31). We found that among 25 HD patients tested for DNA methylation in this study, the DNA intermediate methylation of the *HES4* promoter is highly correlated with severity of striatal degeneration. Interestingly, this correlation is specific for striatal degeneration, but not cortical degeneration despite that the DNA methylation of *HES4* was assessed in the cortex. The selective correlation between the degree of the intermediate methylation pattern for the *HES4* promoter and striatal degeneration is in agreement with the primary striatal degeneration in HD, and with *HES4* function to control the expression of forebrain neuron-specific transcriptional factor Mash1, and consequently striatal development (50,70). Functional significance of HES4 in development of HD was further supported by increased mutant HTT-induced nuclear aggregates and cell death following shRNA knockdown of *HES4* in human neuroblastoma cells. While our HES4 shRNA data suggest pathological potential of HES4 by promoting mutant HTT aggregation and cell death in cells (and potentially in the human brain), future studies using HES4 shRNA in human stem cells derived from HD patients are needed to establish the causal role of HES4 in HD pathogenesis. Moreover, since mutant HTT produces broad changes in H3K4me3 patterns throughout the brain, we speculate that additional striatum-specific factors (such as striatum-specific HTT-interacting proteins) are recruited to act on the top of H3K4me3 changes to trigger striatal degeneration.

Age-at-onset in HD is variable by as much as 25 years even with the same number of CAG repeats in the *HTT* gene, suggesting that non-genetic factors, such as the epigenetic factors identified here, may play a role here. Supporting this possibility, we found that there was a strong correlation between DNA intermediate methylation on the *HES4* promoter and age-of-onset of HD. Importantly, this correlation is independent of CAG repeat, indicating that *HES4* may represent an epigenetic modifier of HD. Therefore, it is reasonable to speculate that certain environmental exposures alter DNA methylation of the *HES4* promoter, leading to abnormal HES targeted gene expression in some individuals. Such epigenetic modifications may in turn interact with other genetic susceptibility and facilitate HD pathogenesis. In view of the fact that most promoters are unmethylated in mature tissues including the brain (71,72), methylation of the *HES4* promoter can be considered abnormal and specific to HD pathology although underlying mechanism remains unknown. Our finding identifies the epigenetic modulation of the *HES4* promoter as a potential therapeutic target to postpone HD the age-of-onset. If similar patterns of *HES4* DNA methylation changes in peripheral blood cells are confirmed as in human brains, the *HES4* epigenetic change may also represent a novel biomarker to predict the age-of-onset of the disease.

In summary, our neuron-specific, genome-wide mapping approach identified a large number of epigenetically altered loci in the neuronal HD genome, including loss of H3K4me3 and excessive DNA methylation on the *HES4* promoter, as well as altered expression of *HES4* and its target genes *MASH1* and *P21*. The functional role of HES4 in HD pathogenesis is supported by a significant correlation between *HES4* epigenetic dysregulation

and age-of-onset and striatal degeneration of HD, and by the exacerbation of mutant *HTT*-induced aggregates and cell death after shRNA knockdown of HES4 in human neuroblastoma cells. Our findings implicate imbalances in histone and DNA methylation on *HES4* and other gene promoters as important modifiers of neuronal degeneration and age-of-onset in HD. Thus, epigenetic changes at *HES4* gene may represent a biomarker for predicting clinical and histopathological outcomes and a novel avenue for therapeutic intervention of HD.

Materials and Methods

HD and control brain samples

Fifty-seven postmortem brains, (25 HD and 32 control), were obtained from the Harvard Brain Tissue Resource Center, McLean Hospital (Table 1). All ChIP-sequencing, qPCR and DNA methylation studies were conducted on frozen (never fixed) tissue collected from the rostral dorsolateral portion of the frontal lobe (Brodmann 9). HD brains were selected from a restricted CAG repeat size between 40 and 54 repeats, representative of common repeat sizes in adult onset HD. To increase sample homogeneity (73), each specimen was micro-dissected, avoiding the surface and layer 1 and taking as uniform a sample from the cortical grey matter (II–VI) as possible.

ChIP-seq

Table 1A summarizes the demographics of the six HD and five control brains used for FACS-ChIP sequencing. Postmortem intervals were within the time window in which H3 trimethylation is stable (74–76).

DNA methylation

For DNA methylation analysis, genomic DNA was extracted from 25 HD (including four from ChIP-sequencing) and 27 control brains (Table 1B).

Quantitative reverse-transcriptase polymerase chain reaction

For qRT–PCR, RNA was extracted from a subset of the cohort used for DNA methylation assays (14 HD and 14 control brains, Table 1C).

FACS-ChIP-seq protocol

Neuronal and non-neuronal nuclei were separated (77,78) by fluorescence-based nuclei sorting (FACS), followed by chromatin immunoprecipitation and genome-wide histone methylation mapping via next generation sequencing (ChIP-Seq, see Fig. 1A) (29,76). (i) Nuclei extraction and FACS: ~750 mg of tissue was homogenized in 5 ml of lysis buffer. Lysates were loaded on a sucrose solution and centrifuged at 24 400 rpm for 2.5 h at 4°C. Nuclei pellets were resuspended in 500 μl PBS and incubated in staining mix containing 1:1200 anti-NeuN (Millipore), 1:1400 Alexa488 goat anti-mouse secondary antibody (Invitrogen)] for 45 min. FACS was done at the Boston University Medical School Flow Cytometry Core Lab on a FACSVantage SE flow cytometer. (ii) The sorted nuclei (3–5 million) were digested with micrococcal nuclease (4 U/ml) at 37°C for 5 min. The reaction was stopped and nuclei were lysed and pre-cleared by Protein G Agarose. Chromatin immunoprecipitation was carried out by incubating digested nuclei with anti-H3K4me3 (1:315; Upstate; 07–473) at 4°C overnight. Immunoprecipitated chromatin was incubated with Protein G Agarose for 1 h, and beads were washed by a series of low and high salt buffer, lithium chloride buffer, TE buffer and then eluted in 0.1 M $NaHCO_3$ and 1% SDS. The eluted DNA was digested with proteinase K and then purified. (iii) ChIP-Seq Library Construction was carried out according to the Illumina protocol using Genomic Adaptor Oligo Mix (Illumina) by Fastlink DNA Ligation Kit (Epicentre) the Genomic PCR Primers (Illumina) according to the Illumina protocol. PCR product was cleaned and correct size of PCR product was confirmed by gel electrophoresis. (iv) The smaller smear was gel purified and libraries were sent for deep-sequencing on the Illumina Genome Analyzer of Deep Sequencing core facilities at University of Massachusetts School of Medicine.

Computational analysis of H3 trimethylation landscapes

All sequencing libraries were single-end 36 bp reads which were mapped to the gender appropriate human genome (HG19) by Bowtie (version 0.11.3), allowing up to one mismatch. Reads that mapped to multiple locations were discarded. The MACS software (version 1.3.5) was used to identify statistically enriched H3K4me3 regions (termed 'peaks' hereafter). We contrasted each sample against the input sample using bw = 230 and tsize = 36, and default values for the remaining parameters in MACS. To identify differentially expressed H3K4me3 peaks between controls and HD cases, all peaks were combined and overlapping peaks merged, resulting in 33 148 peaks. H3K4me3 peaks that were significantly decreased in the HD samples were defined as follows: (i) minimum peak size of 1 Kb with pseudo-count 0.001 for average densities; (ii) average read density in control samples ≥0.01, (iii) the ratio of average read densities Control:HD ≥2 and (iv) the t-test *P*-value ≤0.05. A Benjamini Hochberg false discovery rate was calculated. Reciprocal criteria were used to define H3K4me3 peaks significantly increased in HD.

GO term enrichment analysis

We used the getEnrichedGO function in the ChIPpeakAnno R package (79) to test whether certain loci of H3K4me3 (associated with specific genes) were overrepresented than would be expected by chance (adjusted $P < 0.05$, according to Benjamini & Hochberg (1995) step-up FDR controlling procedure).

Phylogenetic analysis of HES family genes

HES gene family and protein sequences were obtained from NCBI and Ensembl databases. Multiple sequence alignment of protein sequences was performed using ClustalW algorithm and edited in GeneDoc program using Blosum62 as similarity scoring matrix.

DNA methylation detection protocol

Genomic DNA (gDNA) was extracted from frozen brain using the Blood & Cell Culture DNA kit (Qiagen) and quantified by NanoDrop 2000 and 0.7% agarose gel electrophoresis for DNA integrity. Samples showing a A260/A280 ratio >1.7 and a major band around 30 kb were included in methylation analysis. DNA methylation was measured by the Methyl-Profiler PCR Array according to manufacturer's instructions (SABiosciences/Qiagen). This assay is based on MethylScreen (80,81) with combined digestion of methylation-sensitive type II enzyme (*HpaII*/*HhaI*) and methylation-dependent type IV enzyme (McrBC) (EpiTect Methyl DNA Restriction kit, Qiagen) followed by real-time PCR analysis of remaining gDNA. Primers were designed, evaluated and provided by SABiosciences/Qiagen for human *HES4 (catalog# MePH00010-2A)*. Briefly, 1 μg of gDNA from each case or control was divided among four digestion-conditions: mock, HpaII/*HhaI*, McrBC and *HpaII*/*HhaI*+ McrBC. Over-night digestion at 37°C with qPCR was

conducted with gene-specific primers for equal quantities (1/25th) of differentially treated genomic DNAs on an ABI Prism 7000 system. Cycle threshold (Ct) values for each condition were used to calculate un-methylated (UM), fully methylated (FM) and intermediately methylated (IM) DNA such that UM, FM and IM sum to 1.0 for a given sample. All experiments and data analyses were done in double blind.

RNA isolation and gene expression analyses (qRT–PCR)

Total RNA was extracted from frozen human HD and control brain with Trizol reagent and cleaned with an RNeasy micro kit (Qiagen). Total RNA was reverse transcribed to cDNA using SuperScript II Reverse Transcriptase Kit (Invitrogen). The qRT–PCR was performed using Taqman Gene Expression Assays on 7500 Real-Time PCR System. Probes and primers specific for human *HES4* and 18S RNA (Hs00368353_g1 and Hs99999901_s1, respectively) were used according to the manufacturer's protocol. Averaged threshold-cycle (Ct) values of the 18S RNA were used to normalize the target gene (*HES4*), which then were used to determine the relative expression of the gene for HD versus control samples by the ΔΔCt method.

To analyze HES4 mRNA in Neu^+ (neuronal) and Neu^- (non-neuronal) nuclei, total RNA was extracted from 1–3 million of FACS sorted human brain nuclei using TRIzol reagent (Invitrogen) according to the manufacturer's protocol. cDNA was synthesized using Script™ cDNA Synthesis Kit (Bio-Rad #170-8891), following the manufacturer's instructions. Quantitative real-time PCR was performed in triplicate by using Power SYBR® Green PCR Master Mix (AB applied biosystem, #4367659) on LightCycler 96 Real-Time PCR System from Roche. The mRNA level was normalized by gene 18 s rRNA. Primers used for HES4 primer set #2: forward TCAGCTCAAAACCCTCATCC, reverse TGTCTCA CGGTCATCTCCAG; HES4 primer set #3: forward ATCCTGGAGA TGACCGTGAG, reverse CGGTACTTGCCCAGAACG; 18s rRNA forward GTTGGTGGAGCGATTTGTCT, reverse GAACGCCACTTG TCCCTCTA.

Electrophoretic mobility shift assay

The promoter region of the *HES4* gene was obtained by cloning the qPCR product of the *HES4* DNA methylation assay into pGEM3zf at the *Hin*cII site followed by DNA sequencing of the insert for confirmation. This qPCR amplicon expands a 269 bp region −387/−118 upstream of the human *HES4* gene TSS. To test its binding capability under different methylation states to nuclear proteins in brain, we excised this fragment from vector using *Eco*RI and *Hind*III, and digested it further with *Bam*HI sites to yield two fragments of identical size (134–135 bp) and then treated the fragments with or without SssI DNA methylase. Complementary genome DNA strands were annealed at room temperature for 30 minutes after heated to 80°C by the following different combinations (i) '*unmethylated*' probe from two strands without treatment of Sssi, (ii) '*methylated*' probe from two strands with treatment of Sssi, (iii) 'hemi-methylated probe' from one strand with treatment of Sssi and one strand without treatment of Sssi. The *Bam*HI-digested, un-/hemi-/fully-methylated double-stranded DNA then were filled in with ^{32}P-labeled dCTP as described previously (82). EMSA was performed as described previously with modifications (82). Briefly, lysate in 20 μg proteins was pre-incubated on ice for 10 min in binding buffer (15 μl volume) before ^{32}P-labeled double-strand probe in 1 ng was added. After 10 min incubation at 23°C reaction mixtures were fractionated on 4% non-denaturing polyacrylamide gel in 0.25 × TBE and autoradiography was completed.

Statistical analysis of the relationship of HES4 DNA methylation with level of striatal involvement and age-of-onset in HD

Twenty-two of the 25 HD samples studied had been evaluated previously for levels of striatal and cortical involvement (31). Briefly, each brain sample was reviewed by gross and microscopic examination for the level of involvement for 50 brain regions. Cluster analysis reduced the data to two main measures of involvement: (i) striatal and (ii) cortical. The striatal cluster represented a synthesis of 28 brain measures and the cortical cluster constituted 13 brain measures. Comparisons between HD cases and controls to assess possible differences in age at death and postmortem interval were analyzed by Student's *t*-test. The relationship of the level of UM, IM or FM to the level of striatal involvement was studied by Spearman correlation, and by a general linear model controlling for the effect of the size of the expanded CAG repeat size and the level of cortical involvement. The *t*-tests, Spearman correlation and general linear models were performed by SAS version 9.3.

HTB-11 cell culture, transfection of shRNA-HES4 and qRT–PCR of HES4 mRNA

HTB-11 cells (SK-N-SH, human neuroblastoma) were obtained from ATCC and cultured in DMEM medium plus 10% fetal bovine serum, glutamine, high glucose and sodium pyruvate. Constructs expressing human HTT fragment (30 amino acid residues at the N-terminus) with varied length (23, 73 or 145) of N-terminal Q repeats in pcDNA3 plasmid were obtained from Coriell Institute for Medical Research via GenScript (Piscataway, NJ). Constructs expressing one control shRNA and four different shRNAs to the human HES4 gene were purchased from Qiagen. Cell transfection was conducted by Lipofectamine 2000 (Life Technologies). Successful transfection was indicated by green fluorescence of GFP expressed by co-transfected shRNA vector.

Twenty-six hours after transfecting with three different amounts of individual shRNA constructs, we extracted total RNAs and converted them into cDNA using SuperScript III kit (Life Technologies). Human HES4 mRNA level was determined by qRT–PCR analysis using the TaqMan kit (Life Technologies) as described previously (83).

Detection of mutant HTT-induced aggregates and cell death in HBT-11 cells

To test the effect of shRNA-HES4 on mutant *HTT*-induced aggregates and cell death, we determined ubiquitin-positive aggregates by immunocytochemistry and cell death by trypan blue exclusion assay for HTB-11 cells cultured on glass surface coated with D-poly-lysine using the protocol described previously (84). HTB-11 cells were transfected with one of four distinct shRNA-HES4 (shRNA-HES4–1, shRNA-HES4–2, shRNA4–3 and shRNA4–4) or scramble shRNA (control shRNA for non-specific and off-target effects) with or without HTT constructs at different ratio for 24 h before. HTB-11 cells were incubated with polyclonal antibody against ubiquitin (Dako, diluted 1:100) at 4°C overnight and visualized by a second antibody conjugated with Cy3. GFP expressed from shRNA constructs was used as indicator of transfection efficiency. Nuclear DNA was highlighted by DAPI staining (1 ng/ml) for 5 min before mounting. Signals of ubiquitin, GFP

and DAPI were collected from cells as described previously using fluorescent microscope (84). Cell death was tested by trypan blue exclusion 40 hrs after transfection, according to the manufacturer protocol (Sigma-Aldrich, St Louis, MO). Briefly, cells were exposed to a mixture of 0.4% trypan blue reagent: HBSS = 1:1 for 5 min at 37°C before cell images were taken for the same view on bright field for blue staining of dying cells, and under fluorescence for GFP (Nikon Eclipse TE200 system equipped with QICAM CCD camera). Cell images at ×10 object lens were taken randomly from triple transfected wells. Blue cells were labeled by Photo Shop software and counted by ImageJ software after alignment of blue cells with GFP positive cells. Each view contained 60~120 GFP-positive cells. Percentage of cell death was calculated by blue cell number against GFP cells. Mean values were further calculated from five views.

Quantitative analysis of HTT aggregates

To assess the effect of HES4 shRNA knockdown, we used an automated using ImageJ version 1.49 g analysis with a custom script for analysis of HTT aggregation in cells stained with ubiquitin after transfection with HTT and shRNA. Non-cellular background was first removed from the ubiquitin-RFP image using Gaussian blur with a sigma of 20, thresholding by mean signal. Next, the cellular area was identified based on the mask. Each selected area was separately analyzed and using 'max entropy' thresholding, particles 10^2 pixels or greater were counted as an aggregate. We quantified the relative size of cellular aggregates by calculating from the proportion of the aggregate to the cellular area being assessed. We quantified the density of aggregation by the measurement of pixel intensity, which was calculated by multiplying the total aggregate area by the mean signal intensity. Unequal variance Welch's *t*-tests were used to assess statistical differences in protein aggregation between different HTT cotransfected with sc shRNA or HES4 shRNA.

Authors' Contributions

(i) Conducted experiments (I.C., M.J., J.E.C., P.L., Y.W., Y.J.: nuclei sorting and ChIP-seq assays; G.B., K.P., M.Z.: DNA methylation assays, HTB-11 HES4 knock-down, Ubiquitin/HTT aggregates, cell death, EMSA; P.L., Y.W., Y.J.: EMSA, RNA quantification and qPCR assays); (ii) bioinformatical analyses (H.S., X.D., A.G., E.R., Z.W.); (iii) provided resources and materials (R.H.M., S.A.); (iv) designed the study and wrote the paper (J.F.-C., R.H.M., Z.W., S.A., G.B.).

Supplementary Material

Supplementary Material is available at *HMG* online.

Conflict of Interest statement. None declared.

Funding

This work was supported by the National Institutes of Health (1R01NS073947 Epigenetic Markers in Huntington's disease Brain, NS041083-07, R21NS076958) and The Jerry McDonald Huntington's Disease Research Fund. We thank Adam Labadorf for his analysis of the correlation between HES4 mRNA and striatal degeneration score in HD brains.

References

1. Martin, J.B. and Gusella, J.F. (1986) Huntington's disease. Pathogenesis and management. *N. Engl. J. Med.*, **315**, 1267–1276.
2. Vonsattel, J.P. and DiFiglia, M. (1998) Huntington disease. *J. Neuropathol. Exp. Neurol.*, **57**, 369–384.
3. Group, T.H.s.D.C.R. (1993) A novel gene containing a trinucleotide repeat that is expanded and unstable on Huntington's disease chromosomes. The Huntington's Disease Collaborative Research Group. *Cell*, **72**, 971–983.
4. MacDonald, M.E., Gines, S., Gusella, J.F. and Wheeler, V.C. (2003) Huntington's disease. *Neuromol. Med.*, **4**, 7–20.
5. Gusella, J.F. and MacDonald, M.E. (2009) Huntington's disease: the case for genetic modifiers. *Genome Med.*, **1**, 80.
6. Djousse, L., Knowlton, B., Hayden, M., Almqvist, E.W., Brinkman, R., Ross, C., Margolis, R., Rosenblatt, A., Durr, A., Dode, C. *et al.* (2003) Interaction of normal and expanded CAG repeat sizes influences age at onset of Huntington disease. *Am. J. Med. Genet. A*, **119A**, 279–282.
7. Cha, J.H. (2000) Transcriptional dysregulation in Huntington's disease. *Trends Neurosci.*, **23**, 387–392.
8. Dunah, A.W., Jeong, H., Griffin, A., Kim, Y.M., Standaert, D.G., Hersch, S.M., Mouradian, M.M., Young, A.B., Tanese, N. and Krainc, D. (2002) Sp1 and TAFII130 transcriptional activity disrupted in early Huntington's disease. *Science*, **296**, 2238–2243.
9. Vashishtha, M., Ng, C.W., Yildirim, F., Gipson, T.A., Kratter, I. H., Bodai, L., Song, W., Lau, A., Labadorf, A., Vogel-Ciernia, A. *et al.* (2013) Targeting H3K4 trimethylation in Huntington disease. *Proc. Natl Acad. Sci. USA*, **110**, E3027–E3036.
10. Jakovcevski, M. and Akbarian, S. (2012) Epigenetic mechanisms in neurological disease. *Nat. Med.*, **18**, 1194–1204.
11. Steffan, J.S., Bodai, L., Pallos, J., Poelman, M., McCampbell, A., Apostol, B.L., Kazantsev, A., Schmidt, E., Zhu, Y.Z., Greenwald, M. *et al.* (2001) Histone deacetylase inhibitors arrest polyglutamine-dependent neurodegeneration in Drosophila. *Nature*, **413**, 739–743.
12. Steffan, J.S., Kazantsev, A., Spasic-Boskovic, O., Greenwald, M., Zhu, Y.Z., Gohler, H., Wanker, E.E., Bates, G.P., Housman, D.E. and Thompson, L.M. (2000) The Huntington's disease protein interacts with p53 and CREB-binding protein and represses transcription. *Proc. Natl Acad. Sci. USA*, **97**, 6763–6768.
13. Dompierre, J.P., Godin, J.D., Charrin, B.C., Cordelieres, F.P., King, S.J., Humbert, S. and Saudou, F. (2007) Histone deacetylase 6 inhibition compensates for the transport deficit in Huntington's disease by increasing tubulin acetylation. *J. Neurosci.: the Official Journal of the Society for Neuroscience*, **27**, 3571–3583.
14. Ferrante, R.J., Kubilus, J.K., Lee, J., Ryu, H., Beesen, A., Zucker, B., Smith, K., Kowall, N.W., Ratan, R.R., Luthi-Carter, R. *et al.* (2003) Histone deacetylase inhibition by sodium butyrate chemotherapy ameliorates the neurodegenerative phenotype in Huntington's disease mice. *J. Neurosci.: the Official Journal of the Society for Neuroscience*, **23**, 9418–9427.
15. Ryu, H., Lee, J., Olofsson, B.A., Mwidau, A., Deodeoglu, A., Escudero, M., Flemington, E., Azizkhan-Clifford, J., Ferrante, R.J. and Ratan, R.R. (2003) Histone deacetylase inhibitors prevent oxidative neuronal death independent of expanded polyglutamine repeats via an Sp1-dependent pathway. *Proc. Natl Acad. Sci. USA*, **100**, 4281–4286.
16. Thomas, E.A., Coppola, G., Desplats, P.A., Tang, B., Soragni, E., Burnett, R., Gao, F., Fitzgerald, K.M., Borok, J.F., Herman, D. *et al.* (2008) The HDAC inhibitor 4b ameliorates the disease phenotype and transcriptional abnormalities in Huntington's disease transgenic mice. *Proc. Natl Acad. Sci. USA*, **105**, 15564–15569.

17. Goula, A.V., Stys, A., Chan, J.P., Trottier, Y., Festenstein, R. and Merienne, K. (2012) Transcription elongation and tissue-specific somatic CAG instability. *PLoS Genet.*, **8**, e1003051.
18. Sun, X.J., Wei, J., Wu, X.Y., Hu, M., Wang, L., Wang, H.H., Zhang, Q.H., Chen, S.J., Huang, Q.H. and Chen, Z. (2005) Identification and characterization of a novel human histone H3 lysine 36-specific methyltransferase. *J. Biol. Chem.*, **280**, 35261–35271.
19. Seong, I.S., Woda, J.M., Song, J.J., Lloret, A., Abeyrathne, P.D., Woo, C.J., Gregory, G., Lee, J.M., Wheeler, V.C., Walz, T. *et al.* (2010) Huntingtin facilitates polycomb repressive complex 2. *Hum. Mol. Genet.*, **19**, 573–583.
20. Lee, J., Hong, Y.K., Jeon, G.S., Hwang, Y.J., Kim, K.Y., Seong, K.H., Jung, M.K., Picketts, D.J., Kowall, N.W., Cho, K.S. *et al.* (2012) ATRX induction by mutant huntingtin via Cdx2 modulates heterochromatin condensation and pathology in Huntington's disease. *Cell Death Diff.*, **19**, 1109–1116.
21. Ryu, H., Lee, J., Hagerty, S.W., Soh, B.Y., McAlpin, S.E., Cormier, K.A., Smith, K.M. and Ferrante, R.J. (2006) ESET/SETDB1 gene expression and histone H3 (K9) trimethylation in Huntington's disease. *Proc. Natl Acad. Sci. USA*, **103**, 19176–19181.
22. Ruthenburg, A.J., Allis, C.D. and Wysocka, J. (2007) Methylation of lysine 4 on histone H3: intricacy of writing and reading a single epigenetic mark. *Mol. Cell.*, **25**, 15–30.
23. Li, B., Carey, M. and Workman, J.L. (2007) The role of chromatin during transcription. *Cell*, **128**, 707–719.
24. Guttman, M., Amit, I., Garber, M., French, C., Lin, M.F., Feldser, D., Huarte, M., Zuk, O., Carey, B.W., Cassady, J.P. *et al.* (2009) Chromatin signature reveals over a thousand highly conserved large non-coding RNAs in mammals. *Nature*, **458**, 223–227.
25. Pan, G., Tian, S., Nie, J., Yang, C., Ruotti, V., Wei, H., Jonsdottir, G.A., Stewart, R. and Thomson, J.A. (2007) Whole-genome analysis of histone H3 lysine 4 and lysine 27 methylation in human embryonic stem cells. *Cell. Stem Cell*, **1**, 299–312.
26. Santos-Rosa, H., Schneider, R., Bannister, A.J., Sherriff, J., Bernstein, B.E., Emre, N.C., Schreiber, S.L., Mellor, J. and Kouzarides, T. (2002) Active genes are tri-methylated at K4 of histone H3. *Nature*, **419**, 407–411.
27. Zhou, V.W., Goren, A. and Bernstein, B.E. (2011) Charting histone modifications and the functional organization of mammalian genomes. *Nat. Rev. Genetics*, **12**, 7–18.
28. Han, I., You, Y., Kordower, J.H., Brady, S.T. and Morfini, G.A. (2010) Differential vulnerability of neurons in Huntington's disease: the role of cell type-specific features. *J. Neurochem.*, **113**, 1073–1091.
29. Cheung, I., Shulha, H.P., Jiang, Y., Matevossian, A., Wang, J., Weng, Z. and Akbarian, S. (2010) Developmental regulation and individual differences of neuronal H3K4me3 epigenomes in the prefrontal cortex. *Proc. Natl Acad. Sci. USA*, **107**, 8824–8829.
30. Myers, R.H., Vonsattel, J.P., Paskevich, P.A., Kiely, D.K., Stevens, T.J., Cupples, L.A., Richardson, E.P. Jr and Bird, E.D. (1991) Decreased neuronal and increased oligodendroglial densities in Huntington's disease caudate nucleus. *J. Neuropathol. Exp. Neurol.*, **50**, 729–742.
31. Hadzi, T.C., Hendricks, A.E., Latourelle, J.C., Lunetta, K.L., Cupples, L.A., Gillis, T., Mysore, J.S., Gusella, J.F., MacDonald, M.E., Myers, R.H. *et al.* (2012) Assessment of cortical and striatal involvement in 523 Huntington disease brains. *Neurology*, **79**, 1708–1715.
32. van Roon-Mom, W.M., Hogg, V.M., Tippett, L.J. and Faull, R.L. (2006) Aggregate distribution in frontal and motor cortex in Huntington's disease brain. *Neuroreport*, **17**, 667–670.
33. Shulha, H.P., Cheung, I., Whittle, C., Wang, J., Virgil, D., Lin, C. L., Guo, Y., Lessard, A., Akbarian, S. and Weng, Z. (2012) Epigenetic signatures of autism: trimethylated H3K4 landscapes in prefrontal neurons. *Arch. Gen. Psychiatr.*, **69**, 314–324.
34. Thathiah, A., Horre, K., Snellinx, A., Vandewyer, E., Huang, Y., Ciesielska, M., De Kloe, G., Munck, S. and De Strooper, B. (2013) beta-arrestin 2 regulates Abeta generation and gamma-secretase activity in Alzheimer's disease. *Nat. Med.*, **19**, 43–49.
35. Peachey, N.S., Ray, T.A., Florijn, R., Rowe, L.B., Sjoerdsma, T., Contreras-Alcantara, S., Baba, K., Tosini, G., Pozdeyev, N., Iuvone, P.M. *et al.* (2012) GPR179 is required for depolarizing bipolar cell function and is mutated in autosomal-recessive complete congenital stationary night blindness. *Am. J. Hum. Genet.*, **90**, 331–339.
36. Rodriguez, P.Q., Lohkamp, B., Celsi, G., Mache, C.J., Auer-Grumbach, M., Wernerson, A., Hamajima, N., Tryggvason, K. and Patrakka, J. (2013) Novel INF2 mutation p. L77P in a family with glomerulopathy and Charcot-Marie-Tooth neuropathy. *Pediatr. Nephrol.*, **28**, 339–343.
37. Paciorkowski, A.R. and Darras, B.T. (2013) Making sense of genetic heterogeneity: emergence of pathways in developmental brain disorders. *Neurology*, **80**, 426–427.
38. Wood, H.B. (2010) TMEM106B is a susceptibility locus for Ftld. *Nat. Rev. Neurology*, **6**, 184.
39. Finch, N., Carrasquillo, M.M., Baker, M., Rutherford, N.J., Coppola, G., Dejesus-Hernandez, M., Crook, R., Hunter, T., Ghidoni, R., Benussi, L. *et al.* (2011) TMEM106B regulates progranulin levels and the penetrance of FTLD in GRN mutation carriers. *Neurology*, **76**, 467–474.
40. Rutherford, N.J., Carrasquillo, M.M., Li, M., Bisceglio, G., Menke, J., Josephs, K.A., Parisi, J.E., Petersen, R.C., Graff-Radford, N.R., Younkin, S.G. *et al.* (2012) TMEM106B risk variant is implicated in the pathologic presentation of Alzheimer disease. *Neurology*, **79**, 717–718.
41. O'Keeffe, G.W., Gutierrez, H., Pandolfi, P.P., Riccardi, C. and Davies, A.M. (2008) NGF-promoted axon growth and target innervation requires GITRL-GITR signaling. *Nat. Neurosci.*, **11**, 135–142.
42. Xu, L.G., Li, L.Y. and Shu, H.B. (2004) TRAF7 potentiates MEKK3-induced AP1 and CHOP activation and induces apoptosis. J. Biol. Chem., **279**, 17278–17282.
43. El Yakoubi, W., Borday, C., Hamdache, J., Parain, K., Tran, H.T., Vleminckx, K., Perron, M. and Locker, M. (2012) Hes4 controls proliferative properties of neural stem cells during retinal ontogenesis. *Stem Cells*, **30**, 2784–2795.
44. Rabadan, M.A., Cayuso, J., Le Dreau, G., Cruz, C., Barzi, M., Pons, S., Briscoe, J. and Marti, E. (2012) Jagged2 controls the generation of motor neuron and oligodendrocyte progenitors in the ventral spinal cord. *Cell Death Diff.*, **19**, 209–219.
45. Hodges, A., Strand, A.D., Aragaki, A.K., Kuhn, A., Sengstag, T., Hughes, G., Elliston, L.A., Hartog, C., Goldstein, D.R., Thu, D. *et al.* (2006) Regional and cellular gene expression changes in human Huntington's disease brain. *Human Molecular Genet.*, **15**, 965–977.
46. Kageyama, R., Ohtsuka, T. and Kobayashi, T. (2008) Roles of Hes genes in neural development. *Dev. Growth Diff.*, **50** (Suppl. 1), S97–103.
47. Bertrand, N., Castro, D.S. and Guillemot, F. (2002) Proneural genes and the specification of neural cell types. *Nat. Rev. Neuroscience*, **3**, 517–530.
48. Jhas, S., Ciura, S., Belanger-Jasmin, S., Dong, Z., Llamosas, E., Theriault, F.M., Joachim, K., Tang, Y., Liu, L., Liu, J. *et al.* (2006)

Hes6 inhibits astrocyte differentiation and promotes neurogenesis through different mechanisms. *J. Neurosci.*, **26**, 11061–11071.
49. Maunakea, A.K., Nagarajan, R.P., Bilenky, M., Ballinger, T.J., D'Souza, C., Fouse, S.D., Johnson, B.E., Hong, C., Nielsen, C., Zhao, Y. *et al.* (2010) Conserved role of intragenic DNA methylation in regulating alternative promoters. *Nature*, **466**, 253–257.
50. Casarosa, S., Fode, C. and Guillemot, F. (1999) Mash1 regulates neurogenesis in the ventral telencephalon. *Development*, **126**, 525–534.
51. Diguet, E., Fernagut, P.O., Scherfler, C., Wenning, G. and Tison, F. (2005) Effects of riluzole on combined MPTP + 3-nitropropionic acid-induced mild to moderate striatonigral degeneration in mice. *J. Neural. Transm.*, **112**, 613–631.
52. Ryman-Rasmussen, J.P., Griffith, A., Oloff, S., Vaidehi, N., Brown, J.T., Goddard, W.A. III and Mailman, R.B. (2007) Functional selectivity of dopamine D1 receptor agonists in regulating the fate of internalized receptors. *Neuropharmacology*, **52**, 562–575.
53. Katritch, V., Cherezov, V. and Stevens, R.C. (2013) Structure-function of the G protein-coupled receptor superfamily. *Ann. Rev. Pharmacol. Toxicol.*, **53**, 531–556.
54. Rajagopal, S., Rajagopal, K. and Lefkowitz, R.J. (2010) Teaching old receptors new tricks: biasing seven-transmembrane receptors. *Nat. Rev. Drug Discovery*, **9**, 373–386.
55. Ooi, L. and Wood, I.C. (2008) Chromatin switching and transcriptional regulation in disease. *Biochem. Soc. Trans.*, **36**, 599–602.
56. Urdinguio, R.G., Sanchez-Mut, J.V. and Esteller, M. (2009) Epigenetic mechanisms in neurological diseases: genes, syndromes, and therapies. *Lancet. Neurol.*, **8**, 1056–1072.
57. Stack, E.C., Del Signore, S.J., Luthi-Carter, R., Soh, B.Y., Goldstein, D.R., Matson, S., Goodrich, S., Markey, A.L., Cormier, K., Hagerty, S.W. *et al.* (2007) Modulation of nucleosome dynamics in Huntington's disease. *Hum. Mol. Genet.*, **16**, 1164–1175.
58. Eidelberg, D. and Surmeier, D.J. (2011) Brain networks in Huntington disease. *J. Clin. Invest.*, **121**, 484–492.
59. Tai, Y.F., Scherfler, C., Brooks, D.J., Sawamoto, N. and Castiello, U. (2004) The human premotor cortex is 'mirror' only for biological actions. *Curr. Biol.*, **14**, 117–120.
60. Brooks, D.J. (1991) Detection of preclinical Parkinson's disease with PET. *Geriatrics*, **46**(Suppl. 1), 25–30.
61. Scherfler, C., Khan, N.L., Pavese, N., Eunson, L., Graham, E., Lees, A.J., Quinn, N.P., Wood, N.W., Brooks, D.J. and Piccini, P.P. (2004) Striatal and cortical pre- and postsynaptic dopaminergic dysfunction in sporadic parkin-linked parkinsonism. *Brain: J. Neurol.*, **127**, 1332–1342.
62. Pasini, D., Hansen, K.H., Christensen, J., Agger, K., Cloos, P.A. and Helin, K. (2008) Coordinated regulation of transcriptional repression by the RBP2 H3K4 demethylase and Polycomb-Repressive Complex 2. *Gene Dev.*, **22**, 1345–1355.
63. Toffolo, E., Rusconi, F., Paganini, L., Tortorici, M., Pilotto, S., Heise, C., Verpelli, C., Tedeschi, G., Maffioli, E., Sala, C. *et al.* (2014) Phosphorylation of neuronal Lysine-Specific Demethylase 1LSD1/KDM1A impairs transcriptional repression by regulating interaction with CoREST and histone deacetylases HDAC1/2. *J. Neurochem.*, **128**, 603–616.
64. Lilja, T., Heldring, N. and Hermanson, O. (2013) Like a rolling histone: epigenetic regulation of neural stem cells and brain development by factors controlling histone acetylation and methylation. *Biochimica et Biophysica Acta*, **1830**, 2354–2360.
65. Audet, M. and Bouvier, M. (2012) Restructuring G-protein-coupled receptor activation. *Cell*, **151**, 14–23.
66. Adams, R.L. and Lindsay, H. (1993) What is hemimethylated DNA? *FEBS Lett.*, **320**, 243–245.
67. Gao, Z.G., Verzijl, D., Zweemer, A., Ye, K., Goblyos, A., Ijzerman, A.P. and Jacobson, K.A. (2011) Functionally biased modulation of A(3) adenosine receptor agonist efficacy and potency by imidazoquinolinamine allosteric enhancers. *Biochem. Pharmacol.*, **82**, 658–668.
68. Verzijl, D. and Ijzerman, A.P. (2011) Functional selectivity of adenosine receptor ligands. *Purinergic Signal.*, **7**, 171–192.
69. Gusella, J.F. and MacDonald, M.E. (2006) Huntington's disease: seeing the pathogenic process through a genetic lens. *Trend Biochem. Sci.*, **31**, 533–540.
70. Cussac, D., Newman-Tancredi, A., Duqueyroix, D., Pasteau, V. and Millan, M.J. (2002) Differential activation of Gq/11 and Gi (3) proteins at 5-hydroxytryptamine(2C) receptors revealed by antibody capture assays: influence of receptor reserve and relationship to agonist-directed trafficking. *Mol. Pharmacol.*, **62**, 578–589.
71. Illingworth, R., Kerr, A., Desousa, D., Jorgensen, H., Ellis, P., Stalker, J., Jackson, D., Clee, C., Plumb, R., Rogers, J. *et al.* (2008) A novel CpG island set identifies tissue-specific methylation at developmental gene loci. *PLoS Biol.*, **6**, e22.
72. Bird, A. (2002) DNA methylation patterns and epigenetic memory. *Gene Dev.*, **16**, 6–21.
73. Petretto, E., Mangion, J., Dickens, N.J., Cook, S.A., Kumaran, M.K., Lu, H., Fischer, J., Maatz, H., Kren, V., Pravenec, M. *et al.* (2006) Heritability and tissue specificity of expression quantitative trait loci. *PLoS Genet.*, **2**, e172.
74. Akbarian, S. and Huang, H.S. (2009) Epigenetic regulation in human brain-focus on histone lysine methylation. *Biol. Psychiatr.*, **65**, 198–203.
75. Huang, H.S., Matevossian, A., Jiang, Y. and Akbarian, S. (2006) Chromatin immunoprecipitation in postmortem brain. *J. Neurosci. Method.*, **156**, 284–292.
76. Huang, H.S., Matevossian, A., Whittle, C., Kim, S.Y., Schumacher, A., Baker, S.P. and Akbarian, S. (2007) Prefrontal dysfunction in schizophrenia involves mixed-lineage leukemia 1-regulated histone methylation at GABAergic gene promoters. *J. Neurosci.*, **27**, 11254–11262.
77. Jiang, Y., Matevossian, A., Huang, H.S., Straubhaar, J. and Akbarian, S. (2008) Isolation of neuronal chromatin from brain tissue. *BMC Neuroscience*, **9**, 42.
78. Matevossian, A. and Akbarian, S. (2008) Neuronal nuclei isolation from human postmortem brain tissue. *J. Visual Exp.*, **20**, e914.
79. Zhu, L.J., Gazin, C., Lawson, N.D., Pagès, H., Lin, S.M., Lapointe, D.S. and Green, M.R. (2010) ChIPpeakAnno: a Bioconductor package to annotate ChIP-seq and ChIP-chip data. *BMC Bioinformatics*, **11**, 237.
80. Holemon, H., Korshunova, Y., Ordway, J.M., Bedell, J.A., Citek, R.W., Lakey, N., Leon, J., Finney, M., McPherson, J.D. and Jeddeloh, J.A. (2007) MethylScreen: DNA methylation density monitoring using quantitative PCR. *BioTechniques*, **43**, 683–693.
81. Brooks, D.J. (1991) The clinical role of PET in cerebrovascular disease. *Neurosurg. Rev.*, **14**, 91–96.
82. Bai, G. and Kusiak, J.W. (1995) Functional analysis of the proximal 5′-flanking region of the N-methyl-D-aspartate receptor subunit gene, NMDAR1. *J. Biol. Chem.*, **270**, 7737–7744.
83. Bai, G., Ambalavanar, R., Wei, D. and Dessem, D. (2007) Down-regulation of selective microRNAs in trigeminal ganglion neurons following inflammatory muscle pain. *Mol. Pain*, **3**, 15.
84. Jiang, W., Zhang, Y., Xiao, L., Van Cleemput, J., Ji, S., Bai, G. and Zhang, X. (2005) Cannabinoids promote embryonic and adult hippocampus neurogenesis and produce anxiolytic- and antidepressant-like effects. *J. Clin. Invest.*, **115**, 3104–3116.